NUREG/CR-1408
ANL-80-14

NUREG/CR-1408
ANL-80-14

INSTRUMENTED IMPACT PROPERTIES OF ZIRCALOY-OXYGEN AND ZIRCALOY-HYDROGEN ALLOYS

by

A. M. Garde and T. F. Kassner

ARGONNE NATIONAL LABORATORY, ARGONNE, ILLINOIS

Prepared for the U. S. NUCLEAR REGULATORY COMMISSION
under Interagency Agreement DOE 40-550-75

Available from

GPO Sales Program
Division of Technical Information and Document Control
U. S. Nuclear Regulatory Commission
Washington, D.C. 20555

and

National Technical Information Service
Springfield, Virginia 22161

NUREG/CR-1408
ANL-80-14

(Distribution
Code: R3)

ARGONNE NATIONAL LABORATORY
9700 South Cass Avenue
Argonne, Illinois 60439

INSTRUMENTED IMPACT PROPERTIES OF ZIRCALOY-OXYGEN AND ZIRCALOY-HYDROGEN ALLOYS

by

A. M. Garde and T. F. Kassner

Materials Science Division

April 1980

Prepared for the Division of Reactor Safety Research
Office of Nuclear Regulatory Research
U. S. Nuclear Regulatory Commission
Washington, D.C. 20555
Under Interagency Agreement DOE 40-550-75

NRC FIN No. A2017

INSTRUMENTED IMPACT PROPERTIES OF ZIRCALOY-OXYGEN AND ZIRCALOY-HYDROGEN ALLOYS

by

A. M. Garde and T. F. Kassner

ABSTRACT

Instrumented-impact tests were performed on subsize Charpy specimens of Zircaloy-2 and -4 with up to ~1.3 wt % oxygen and ~2500 wt ppm hydrogen at temperatures between 373 and 823 K. Self-consistent criteria for the ductile-to-brittle transition, based upon a total absorbed energy of ~1.3 x 10^4 J/m^2, a dynamic fracture toughness of ~10 MPa·$m^{1/2}$, and a ductility index of ~0, were established relative to the temperature and oxygen concentration of the transformed β-phase material. The effect of hydrogen concentration and hydride morphology, produced by cooling Zircaloy-2 specimens through the temperature range of the $\beta \rightarrow \alpha' +$ hydride phase transformation at ~0.3 and 3 K/s, on the impact properties was determined at temperatures between 373 and 673 K. On an atom fraction basis, oxygen has a greater effect than hydrogen on the impact properties of Zircaloy at temperatures between ~400 and 600 K.

NRC FIN No. | FIN Title

A2017 | Mechanical Properties of Zircaloy

TABLE OF CONTENTS

	Page
ABSTRACT	ii
EXECUTIVE SUMMARY	ix
I. INTRODUCTION	x
II. MATERIALS, APPARATUS, AND EXPERIMENTAL METHODS	1
A. Materials	1
B. Impact Specimen Geometry	1
C. Preparation of Zircaloy-Oxygen and Zircaloy-Hydrogen Specimens	2
1. Oxygen Charging and Homogenization	2
2. Hydrogen Charging and Homogenization	4
D. Impact Testing Facility and Test Procedures	5
1. Impact-testing System	5
2. Impact-testing and Calibration Methods	7
E. Microstructural Evaluations	9
F. Impact Data Analysis	9
III. RESULTS	12
A. Impact Properties of Zircaloy-Oxygen Alloys	12
B. Impact Properties of Zircaloy-Hydrogen Alloys	23
C. Comparison of the Embrittlement Characteristics of Oxygen and Hydrogen	32
IV. SUMMARY AND CONCLUSIONS	34
APPENDICES	
A. Analysis of Uncertainties in the Experimental Data	35
B. Summary of Impact-test Data	37
ACKNOWLEDGMENTS	47
REFERENCES	47

LIST OF FIGURES

No.	Title	Page
1.	Drop-tower Impact-testing Apparatus	5
2.	Block Diagram for Data-readout System of Instrumented Impact-testing System.	6
3.	Anvil Region of Impact-testing System Showing Specimen, Tup, and Pneumatic Clamps That Grip the Specimen during Resistance Heating	6
4.	Anvil Region of Impact-testing System Showing Pneumatic Specimen Clamps in Closed Position	7
5.	Nondimensional Plot of the Compliance C_s of Zircaloy-4 Subsize Charpy Specimens at 298 K as a Function of the Crack Length to Specimen Width Ratio (a/W), Where E and B Are Young's Modulus and the Specimen Thickness, Respectively	8
6.	Load-vs-Time Record for a Typical Linear-elastic Type Fracture of a Zircaloy-4 Specimen with 0.63 wt % Oxygen at 298 K	9
7.	Load-vs-time Record for a Typical Elastic-plastic Type Fracture of an As-received Zircaloy-4 Specimen (0.14 wt % Oxygen) at 296 K	9
8.	Effect of Oxygen Concentration on Maximum Load for Notched and Precracked Zircaloy-2 and -4 Specimens with Longitudinal and Transverse Textures at Temperatures of (a) 373, (b) 473, (c) 673, and (d) 823 K	12
9.	Effect of Temperature on Maximum Load for Homogeneous Zircaloy-Oxygen Alloys with (a) 0.13, (b) 0.45, (c) 0.62 and 0.77, and (d) 0.95 wt % Oxygen	13
10.	Effect of Oxygen Concentration on Crack Initiation Energy per Unit Area for Homogeneous Zircaloy-2 and -4 Specimens with Longitudinal and Transverse Texture at Temperatures of (a) 373, (b) 473, (c) 673 and (d) 823 K	15
11.	Effect of Temperature on Crack Initiation Energy per Unit Area for Transverse Zircaloy-4 Specimens with Oxygen Concentrations between 0.13 and 0.95 wt %.	16
12.	Dependence of Crack Initiation Energy per Unit Area on Temperature for Homogeneous Zircaloy-2 and -4 Specimens with (a) 0.75 and (b) 0.95 wt % Oxygen	16
13.	Effect of Oxygen Concentration on Crack Propagation Energy per Unit Area of Homogeneous Zircaloy-2 and -4 Specimens with Longitudinal and Transverse Textures at Temperatures of (a) 373, (b) 473 and (c) 673 K	17

LIST OF FIGURES

No.	Title	Page
14.	Total Absorbed Energy per Unit Area as a Function of Oxygen Concentration of Homogeneous Zircaloy-2 and -4 Specimens with Longitudinal and Transverse Textures at Temperatures of (a) 373, (b) 473, (c) 673, and (d) 823 K	18
15.	Ductility Index as a Function of Oxygen Concentration of Homogeneous Zircaloy-2 and -4 Specimens at Temperatures of (a) 373 and (b) 473 K.	19
16.	Dynamic Fracture Toughness as a Function of Oxygen Concentration of Homogeneous Zircaloy-2 and -4 Specimens with Longitudinal and Transverse Textures at Temperatures of (a) 373, (b) 473, (c) 673, and (d) 823 K	20
17.	Effect of Temperature on Dynamic Fracture Toughness of Homogeneous Zircaloy-2 and -4 Specimens Containing (a) 0.45 and (b) 0.95 wt % Oxygen	21
18.	SEM Fractographs of Homogeneous Zircaloy-4 Specimens with 0.75 wt % Oxygen Fractured at (a) 373, (b) 473, (c) 673, and (d) 823 K	22
19.	SEM Fractographs of Homogeneous Zircaloy-4 Specimens with (a) 0.62 and (b) 1.10 wt % Oxygen Fractured at 373 and 473 K, Respectively	23
20.	Ductile-to-brittle Transition as a Function of Temperature and Oxygen Concentration of Homogeneous Zircaloy-2 and -4 Alloys Based upon the Following Criteria: (a) Total Absorbed Energy of ~1.3×10^4 J/m^2, (b) Dynamic Fracture Toughness of ~10 MPa·m$^{1/2}$, (c) Ductility Index of ~0, (d) and <25% of the Fracture Surface Area Exhibiting Shear Dimples, and (e) Deflection Angle of the Deformed Specimens of <5°	24
21.	Maximum Load as a Function of Hydrogen Concentration of Zircaloy-2 Specimens with Longitudinal Texture at Several Temperatures between 373 and 673 K	25
22.	Crack Initiation Energy per Unit Area as a Function of Hydrogen Concentration in Zircaloy-2 Specimens at Several Temperatures between 373 and 673 K	26
23.	Crack Propagation Energy per Unit Area as a Function of Hydrogen Concentration in Zircaloy-2 Specimens at Several Temperatures between 373 and 573 K	27
24.	Total Absorbed Energy per Unit Area as a Function of Hydrogen Concentration in Zircaloy-2 Specimens at Temperatures between 373 and 573 K	27

LIST OF FIGURES

No.	Title	Page
25.	Ductility Index of Zircaloy-2 Specimens as a Function of Hydrogen Concentration at Temperatures of 373, 473 and 573 K . . .	28
26.	Dynamic Fracture Toughness as a Function of Hydrogen Concentration in Zircaloy-2 Specimens with Longitudinal Texture at Several Temperatures between 373 and 673 K.	29
27.	SEM Fractographs of Longitudinal Zircaloy-2 Specimens with 600 wt ppm Hydrogen Which Indicate a Predominantly Brittle Fracture Mode after Impact Testing at (a) 373 and (b) 473 K	29
28.	Optical Micrograph of a Zircaloy-2 Specimen with 1000 wt ppm Hydrogen Which Shows Hydride Precipitation at the Periphery of the α' Grains	30
29.	Optical Micrograph of a Zircaloy-2 Specimen with 600 wt ppm Hydrogen Which Shows a Fracture Path along the Periphery of the α' Grains.	30
30.	Optical Micrograph of a Zircaloy-2 Specimen with 227 wt ppm Hydrogen Which Does Not Show Cracks along the Periphery of the α' Grains.	31
31.	SEM Micrograph of the Zircaloy-2 Specimen Depicted in Figs. 27a and 29 (600 wt ppm Hydrogen, 0.3 K/s) That Shows Fracture of Thick Hydride Plates by Deformation Twins in the Metal.	31
32.	SEM Micrograph of the Zircaloy-2 Specimen Depicted in Fig. 30 (227 wt ppm Hydrogen, 3 K/s) That Shows a Fine, Discontinuous Hydride Morphology	31
33.	Comparison of the Effect of Oxygen and Hydrogen on the Dynamic Fracture Toughness of Zircaloy at Temperatures of ≤400 and 600 K, Respectively	32
34.	Three-dimensional Representation of the Plastic Deflection to Maximum Load at 300 K Relative to the β-layer Centerline Oxygen Concentration and Hydrogen Content of Zircaloy-4 Cladding. .	33

LIST OF TABLES

No.	Title	Page
I.	Characteristics of Zircaloy-2 and -4 Materials for Fabrication of Impact Specimens	1
II.	Oxygen-charging and Homogenization Conditions for Zircaloy Subsize Charpy Impact Specimens	3
III.	Hydrogen-charging Conditions for Zircaloy Subsize Charpy Impact Specimens	4
B.1.	Impact Results from Homogeneous Zircaloy-4/Oxygen Specimens with Transverse Texture	38
B.2.	Impact Results from Precracked Zircaloy-4/Oxygen Specimens with Transverse Texture	39
B.3.	Impact Results from Homogeneous Zircaloy-4/Oxygen Specimens with Longitudinal Texture	40
B.4.	Impact Results from Homogeneous Zircaloy-2/Oxygen Specimens with Transverse Texture	41
B.5.	Impact Results from Homogeneous Zircaloy-2/Oxygen Specimens with Longitudinal Texture	42
B.6.	Impact Results from Longitudinal-texture Zircaloy-4 Specimens in As-received Condition and after Cooling through the Temperature Range of the $\beta \rightarrow \alpha'$ Phase Transformation at a Rate of ~3 K/s	43
B.7.	Impact Results from As-received Zircaloy-2 Specimens (0.13 wt % Oxygen) with Longitudinal and Transverse Textures	44
B.8.	Impact Results from Longitudinal-texture Zircaloy-2/Hydrogen Specimens Which Were Cooled through the Temperature Range of the $\beta \rightarrow \alpha'$ + Hydride Phase Transformation at a Rate of ~3 K/s	45
B.9.	Impact Results from Longitudinal-texture Zircaloy-2/Hydrogen Specimens Which Were Cooled through the Temperature Range of the $\beta \rightarrow \alpha'$ Hydride Phase Transformation at a Rate of ~0.3 K/s	46

INSTRUMENTED IMPACT PROPERTIES OF ZIRCALOY-OXYGEN AND ZIRCALOY-HYDROGEN ALLOYS

by

A. M. Garde and T. F. Kassner

EXECUTIVE SUMMARY

The impact properties of Zircaloy with ~0.13 to 1.3 wt % oxygen and ~10 to 2500 wt ppm hydrogen have been evaluated at temperatures between 373 and 823 K. Self-consistent criteria for the transition from ductile to brittle fracture relative to the temperature and oxygen concentration of the material were established on the basis of (a) total absorbed energy of ~1.3×10^4 J/m^2, (b) dynamic fracture toughness of ~10 MPa·m$^{1/2}$, (c) ductility index of ~0, (d) <25% of the fracture surface area exhibiting shear dimples, and (e) deflection angle of the deformed specimens of <5°. The type of alloy (e.g., Zircaloy-2 or -4), texture (i.e., specimen orientation in relation to the rolling direction of the material), and specimen geometry (notch versus fatigue precrack) had virtually no effect on the total absorbed energy and dynamic fracture toughness of specimens which exhibit a predominantly brittle fracture mode.

The influence of hydrogen concentration and the morphology and distribution of the hydride phase, produced by cooling the specimens through the temperature range of the $\beta \rightarrow \alpha'$ + hydride phase transformation at rates of ~0.3 and 3 K/s, on the impact properties of Zircaloy-2 with a longitudinal texture was investigated at temperatures between 373 and 673 K. Hydride precipitation in material cooled at the slower rate occurred primarily at the periphery of the α' grains and the fracture path coincided with this region in specimens that were tested at a low temperature (e.g., 373 K). Dynamic-fracture-toughness values for slow-cooled material with ≥600 wt ppm hydrogen ranged from ~10 to 15 MPa·m$^{1/2}$ at temperatures ≤573 K, whereas the material exhibited large toughness values of ~40-60 MPa·m$^{1/2}$ at 673 K. Because of the fine, discontinuous hydride morphology and transgranular fracture of material that was cooled through the phase-transformation range at the higher rate, the fracture toughness values exhibited a strong dependence on temperature over the range of 373 to 573 K (e.g., ~10-60 MPa·m$^{1/2}$ for Zircaloy with ~1000 wt ppm hydrogen).

Based upon atom fraction, oxygen has a greater effect than hydrogen on the impact properties of transformed β-phase Zircaloy at temperatures between ~400 and 600 K. Consequently, information on the fracture toughness of Zircaloy-oxygen alloys at low temperatures is appropriate for use in analyses of the structural integrity of fuel rods that are subjected to high-temperature oxidation in steam during postulated accident situations in LWRs.

I. INTRODUCTION

Loss-of-coolant accidents (LOCAs) and seismic events can cause transient loads on reactor internals including fuel assemblies. Consequently, mathematical analyses have been performed to evaluate the dynamic response of reactor fuel assemblies subjected to both seismic and LOCA loads.[1-4] The maximum stresses, impact forces, and deflections can be computed and compared with allowable limits to ensure unimpeded insertion of control rods and structural integrity of fuel assemblies from the standpoint of maintaining a coolable geometry. In the initial stages of the LOCA transient, the mechanical properties of undeformed, irradiated Zircaloy fuel cladding are appropriate for use in analytical models. However, if ballooning, rupture, and subsequent oxidation of the fuel cladding occur during the reflood and refill stages of the transient, the geometry and properties of oxidized cladding are relevant to analyses of the structural integrity of fuel assemblies under thermal shock and seismic loads.

Failure boundaries relative to the time-temperature conditions during transient oxidation of ballooned and ruptured cladding have been established for thermal shock as well as impact and compressive loads at low temperatures.[5] This information can be used in evaluations of the margin of performance of emergency core cooling systems in light-water reactors (LWRs); however, the results cannot be incorporated into complex analytical codes which compute stresses, impact forces, and displacements in fuel assemblies during LOCA and seismic events. Information pertaining to the effect of oxidation on the tensile and impact properties of Zircaloy (e.g., modulus of elasticity, ultimate tensile strength, dynamic fracture toughness) coupled with geometric parameters (length, thickness, and diameter of cladding, initial size and distribution of cracks under the oxide layer, orientation of cladding relative to the applied load) can be used with stress-analysis and fracture-mechanics techniques to assess the structural integrity of fuel rods under accident conditions.[6]

This report summarizes results of instrumented impact tests on subsize Charpy specimens of Zircaloy-oxygen and Zircaloy-hydrogen alloys which can be employed along with other property data to determine the response of reactor fuel assemblies to mechanical loads during the latter stages of hypothetical LOCA transients and seismic conditions. Some of the information in this report has appeared in LWR Safety Research Program quarterly progress reports from July 1977 to December 1978.[7-12] The information represents part of the mechanical-property data generated in a U. S. Nuclear Regulatory Commission-sponsored program to determine the influence of oxidation on the tensile[13] and impact properties of Zircaloy as well as the tube-burst,[14] thermal-shock, impact, and diametral-compression properties[5] of Zircaloy cladding.

II. MATERIALS, APPARATUS, AND EXPERIMENTAL METHODS

A. Materials

Table I lists the composition of the Zircaloy-2 and -4 plate obtained from AMAX Specialty Metals, Akron, New York, along with the grain size, thickness, and heat treatment.

TABLE I. Characteristics of Zircaloy-2 and -4 Materials for Fabrication of Impact Specimens

	Zircaloy-2	Zircaloy-4
Composition of As-received Material		
Sn, wt %	1.43	1.40
Fe, wt %	0.13	0.19
Cr, wt %	0.10	0.10
Ni, wt %	0.04	<35 ppm
Al, ppm	<20	<35
B, ppm	<0.2	<0.25
C, ppm	112	<100
Cd, ppm	<0.2	<0.25
Co, ppm	<10	<10
Cu, ppm	<25	<25
Hf, ppm	90	<80
H, ppm	10	-
Mn, ppm	<20	<25
N, ppm	30	-
O, ppm	1290	1400
Si, ppm	32	<60
Ti, ppm	<20	<25
W, ppm	<50	<50
U, ppm	0.025	<1.8
Zr	Balance	Balance
Grain Size, μm	~15	~15
Thickness, mm	6.35	6.35
Specification	ASTM Z-59	ASTM B352-73
Heat Treatment	Hot-rolled and annealed	Hot-rolled and annealed

B. Impact Specimen Geometry

The subsize Charpy specimens (5 mm wide x 5 mm thick x 55 mm long with a 1-mm-deep 45° notch and a 0.25-mm root radius) were fabricated in

accordance with ASTM Standard E23-72. The small specimen size was selected to minimize the time for oxygen diffusion during high-temperature homogenization of the oxidized Zircaloy specimens. However, a valid determination of the plane-strain fracture toughness K_{IC} or the dynamic fracture toughness K_{ID} requires that the basic assumptions of linear-elastic fracture mechanics must be satisfied in the experimental test methods and conditions;[15] e.g., the crack length, thickness, and ligament length must be larger than the plastic zone size, which is proportional to (K_{ID}/σ_{ys}),[2] where σ_{ys} is the yield stress of the material.

Since the properties of Zircaloy-oxygen and Zircaloy-hydrogen alloys which exhibit limited plasticity are of particular interest, the specimen size can be somewhat smaller than for a specimen design based upon the properties of as-received Zircaloy. For example, the calculated plastic zone sizes in as-received material (0.14 wt % oxygen) and a Zircaloy specimen containing 0.7 wt % oxygen are 22.5 and 0.4 mm, respectively, at ~373 K. These values are based upon yield-stress and K_{ID} values of ~300 MPa, 45 MPa·$m^{1/2}$ and ~500 MPa, 10 MPa·$m^{1/2}$ for the respective materials along with the premise that because of the low strain-rate sensitivity[13] (0.03 at room temperature), yield-stress values at a strain rate of ~10^{-3} s^{-1} are appropriate for the higher strain rates encountered under impact loading conditions. From these considerations, it is quite likely that the fracture toughness values for Zircaloy specimens with low concentrations of oxygen and hydrogen at temperatures ≥400 K are larger than the true plane-strain fracture toughness.

Impact tests were performed on notched specimens with and without fatigue precracks. Problems were encountered in producing a planar crack with an a/W ratio of 0.5 (a is the crack length and W is the specimen width) perpendicular to the surface of specimens after oxidation and homogenization at high temperatures. Because of grain growth in the specimens during the long homogenization periods, the crack, which initiates beneath the notch root, frequently propagates along a grain boundary in the transformed β-phase material at an angle other than 90° to the specimen surface. Also, it was very difficult to control propagation of the crack to achieve an a/W ratio of 0.5 with a three-point-bend rotary fatigue precracker. Frequently, specimens with high concentrations of oxygen (≥0.6 wt %) fractured during formation of the fatigue precrack.

Impact tests were performed on both longitudinal and transverse specimens (length parallel and perpendicular to the rolling direction of the plate, respectively) in which the notch was located in the rolling plane.

C. Preparation of Zircaloy-Oxygen and Zircaloy-Hydrogen Specimens

1. Oxygen Charging and Homogenization

The oxidation of Zircaloy at high temperatures results in the formation of a ZrO_2 oxide layer on α-phase Zircaloy below the $\alpha \rightarrow \beta$ phase

transformation temperature of ~1085 K and a $ZrO_2/\alpha/\beta$ composite structure above the transformation temperature (≥1250 K). Thus the test-specimen production scheme essentially consists of two parts: (1) oxidation in steam to the desired oxygen content and (2) homogenization by high-temperature annealing in an inert-gas environment to eliminate the ZrO_2 and α-phase layers and ensure a uniform oxygen concentration in the material.

The impact specimens were degreased in toluene and acetone, dried, and then weighed on a microbalance. Groups of up to eight specimens were suspended inside a silica tube which was evacuated to a pressure of $\sim 4 \times 10^{-2}$ Pa by diffusion and mechanical pumps. A split furnace heated to the desired temperature was placed in contact with the silica tube, which was isolated from the vacuum system, and steam was admitted. After a specified oxidation time, the steam was evacuated from the tube and the furnace was removed to achieve a cooling rate of ~3 K/s through the temperature range of the $\beta \rightarrow \alpha'$ phase transformation. The total oxygen uptake by the specimens was determined from the weight-gain measurements.

Two high-temperature, high-vacuum Centorr furnaces were used for homogenization of the Zircaloy specimens. Both systems have tungsten heating elements and tantalum heat shields and can operate in vacuum, inert-gas, or reducing atmospheres at temperatures up to 1800 K, which were measured with Pt-10% Rh thermocouples and compared with optical-pyrometer and thermal-converter readings. Uniform temperatures were maintained over half the length of the 61-mm-diameter, 125-mm-long and 75-mm-diameter, 200-mm-long heat zones.

The oxygen-charged specimens were suspended by rhenium hooks inside a tantalum capsule, which acted as a getter for residual impurities in the high-purity helium atmosphere. The furnace was evacuated to a pressure of $\sim 4 \times 10^{-3}$ Pa and backfilled with helium several times before heating the furnace to the homogenization temperature. After a specified homogenization time, the specimens were cooled through the temperature range of the $\beta \rightarrow \alpha'$ phase transformation at a rate of ~3 K/s. The time-temperature conditions during oxidation and homogenization are given in Table II.

TABLE II. Oxygen-charging and Homogenization Conditions for Zircaloy Subsize Charpy Impact Specimens

	Oxygen Charging Conditions			Homogenization Conditions		
Material[a]	Temp., K	Time, s	Steam Pressure, Pa	Temp., K	Time, ks	Oxygen, wt %
4L	1273	120	250	1623	453.6	0.44
4L	1283	480	290	1573	516.6	0.73
4L	1293	660	500	1673	331.2	1.05
4T	1174	40	500	1573	388.8	0.29
4T	1303	120	250	1563	489.6	0.59
4T	1278	900	500	1673	331.2	1.00
2L	1283	360	250	1623	334.8	0.73
2L	1275	570	500	1623	437.4	0.82
2L	1296	510	500	1673	432.0	1.00
2T	1273	60	500	1573	491.4	0.68
2T	1283	180	500	1673	428.0	1.00

[a]The symbols 2T, 4T, 2L, and 4L refer to Zircaloy-2 and -4 with transverse and longitudinal textures.

After homogenization, the specimens were reweighed to determine the amount of impurity pickup, the absence of phase boundaries was verified by metallographic observation, and a microhardness profile was obtained across the thickness to ensure that the time was sufficient to produce a uniform oxygen concentration.

2. Hydrogen Charging and Homogenization

The method for producing impact specimens with different hydrogen concentrations was similar to that used for the Zircaloy-oxygen specimens. The notched impact specimens were weighed on a microbalance and groups of up to eight specimens were suspended inside a furnace tube which was attached to a modified Sieverts apparatus. The tube was evacuated to a pressure of $\sim 1.3 \times 10^{-4}$ Pa, the specimens were heated to a temperature in the β-phase region (~1200 K), and a measured quantity of a hydrogen-helium gas mixture (ultrahigh-purity) was admitted to the furnace tube. After a sufficient period for hydrogen absorption and homogenization, the specimens were cooled at controlled rates of 0.3 and 3 K/s to produce different microstructures during the $\beta \rightarrow \alpha' +$ hydride phase transformation. The hydrogen concentration was determined from weight-gain measurements and the values were confirmed by inert-gas fusion analyses of the specimens after impact testing. Typical conditions for producing subsize Charpy-impact specimens with different hydrogen contents are given in Table III.

TABLE III. Hydrogen-charging Conditions for Zircaloy Subsize Charpy Impact Specimens

Temp., K	Initial Pressure of H_2 and He, kPa	Time, ks	Hydrogen, wt ppm
1198	4.0 (H_2) 66.6 (He)	3.6	600
1198	11.2 (H_2) 63.3 (He)	10.8	760
1223	13.6 (H_2) 56.7 (He)	5.4	940
1198	8.0 (H_2) 66.6 (He)	5.4	1000
1198	10.0 (H_2) 63.3 (He)	5.4	1200
1223	20.0 (H_2) 53.3 (He)	5.4	1330

D. Impact Testing Facility and Test Procedures

1. Impact-testing System

A Dynatup Model 8000A drop-weight impact machine with an instrumented tup and data-readout system was purchased from Effects Technology, Inc., Santa Barbara, CA. The drop-weight testing machine can accommodate different specimen sizes and geometries, and the impact velocity and available energy can be varied by altering the drop height and weight of the crosshead. The maximum impact velocity and impact energy obtainable with this machine are 4 m/s and 1.3 kJ, respectively. An optical velocity-measuring device and a digital display system provide the initial and final tup velocities and a value for the absorbed energy during impact. Load- and energy-time data were obtained from an instrumented tup and recorded on a dual-beam storage oscilloscope. The instrumented tup consists of a striking head and a strain gauge with a four-arm semiconductor bridge circuit. The strain gauge, which senses the compressive load on the tup during test-specimen impact, was calibrated by a dynamic loading technique.

Figure 1 shows the testing machine and instrumentation, and Fig. 2 is a schematic diagram[16] of the data-readout system. Figures 3 and 4 show the pneumatic clamps that hold the specimen in position on the anvils. The anvils were electrically insulated from the base plate, and the specimen was heated by resistance heating. Just before impact, the power to the specimen was interrupted, and the clamps were released to remove any constraint on the specimen (i.e., to allow a three-point-bend test configuration). The temperature was controlled and monitored by thermocouples attached to the specimen.

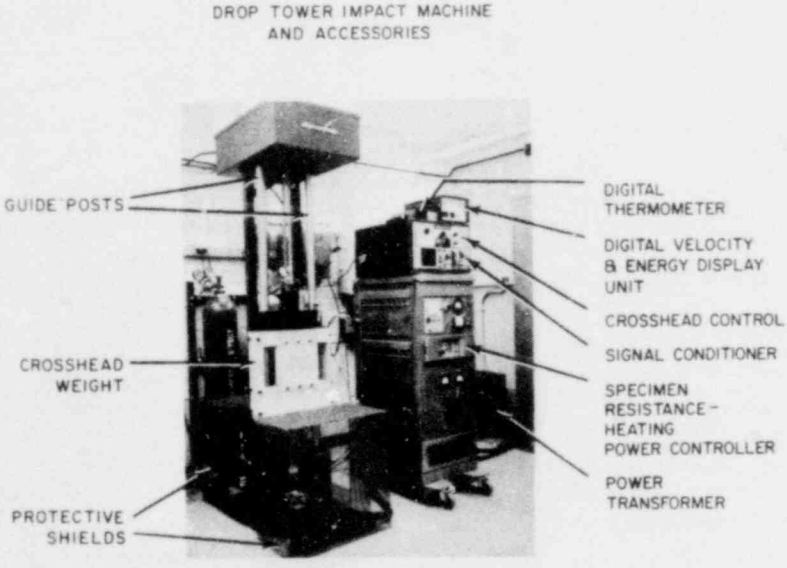

Fig. 1

Drop-tower Impact-testing Apparatus. ANL Neg. No. 306-77-656.

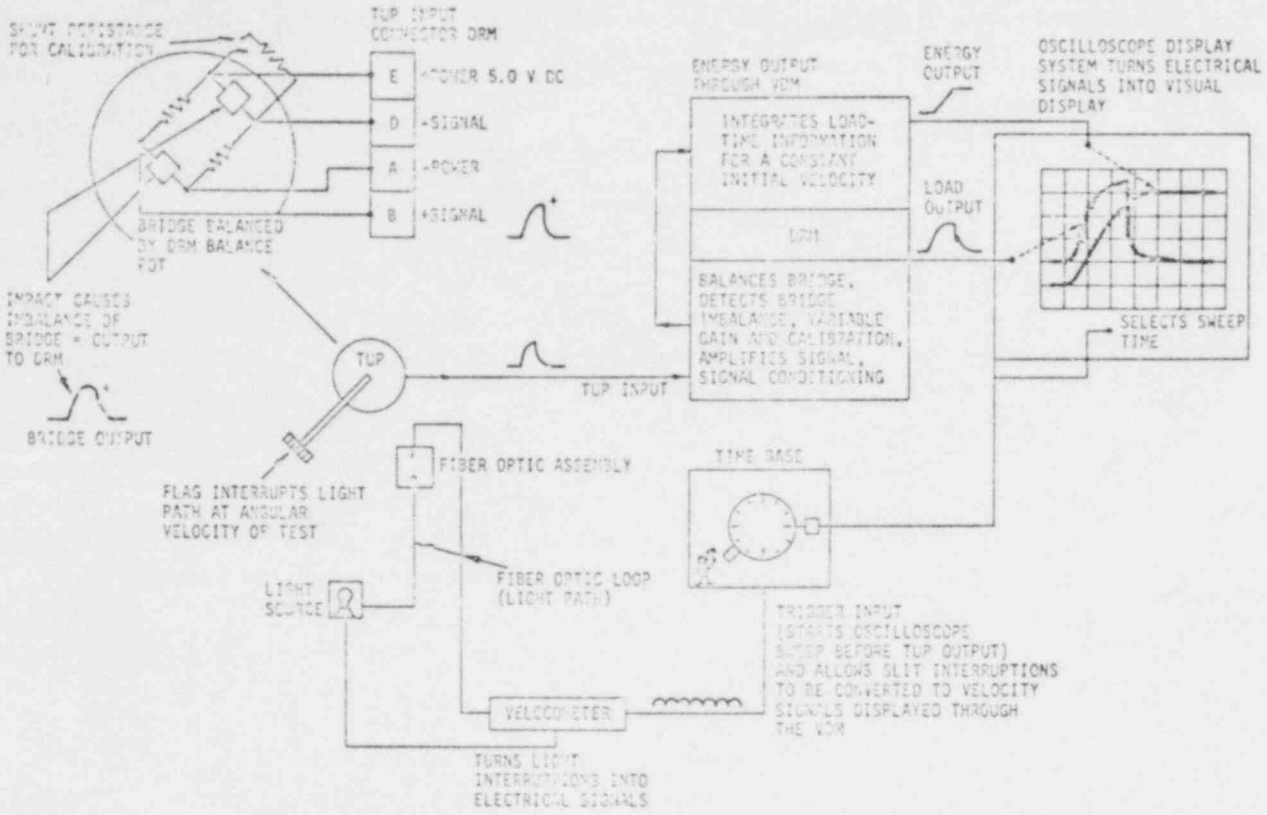

Fig. 2. Block Diagram for Data-readout System of Instrumented Impact-testing System. ANL Neg. No. 306-77-652.

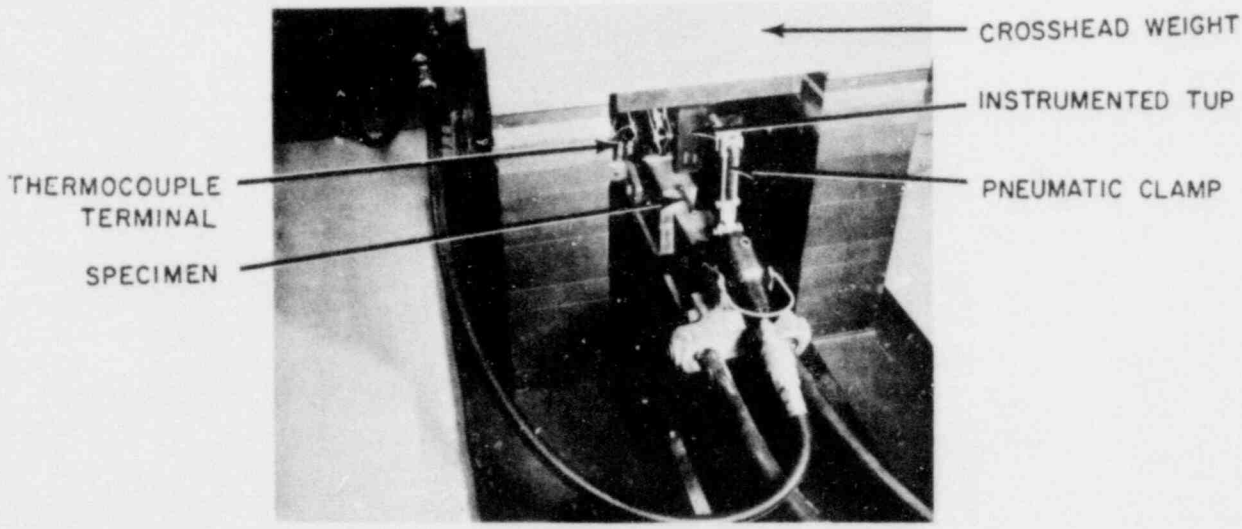

Fig. 3. Anvil Region of Impact-testing System Showing Specimen, Tup, and Pneumatic Clamps That Grip the Specimen during Resistance Heating. Clamps are in the open position. ANL Neg. No. 306-77-655.

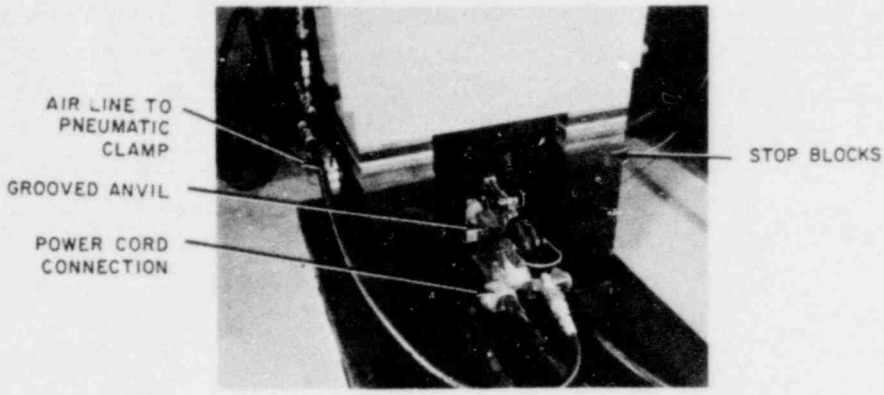

Fig. 4. Anvil Region of Impact-testing System Showing Pneumatic Clamps in Closed Position. Clamps release immediately before impact. ANL Neg. No. 306-77-654.

2. Impact-testing and Calibration Methods

The frequency response of the recorder system sets a lower limit on the total test time and an upper limit on the initial velocity for a valid impact test. The response time ($T_R = 0.35\ f_c$, where f_c is the frequency that yields a 10% attenuation in the signal amplitude) was measured at different levels of sensitivity of the recording system.

Before tests were conducted on the Zircaloy specimens, the instrumented tup and data-readout instrumentation were calibrated by fracturing standard Charpy V-notch specimens fabricated from 6061-T6 aluminum and 4340 steel with a hardness of R_C 54.* The load- and energy-versus-time traces during fracture of the aluminum specimens were recorded on the oscilloscope, and the amplifier gain in the unit was adjusted so that the recorded load limit coincided with the load limit for this material (i.e., 7.74 kN). The aluminum alloy (6061-T6) was chosen as a standard because its room-temperature properties are not strain-rate-dependent, i.e., the static and dynamic limit loads do not differ significantly.[17] The linearity of the calibration was established from the results obtained from the 4340 steel specimen, which has a considerably higher limit load. The optical velocimeter system also requires calibration so that the initial and final velocities of the tup can be calculated. The initial velocity was entered into the unit that integrates the load-time signal to produce a value of the impact energy.

The compliance of as-received Zircaloy-4 specimens (0.14 wt % oxygen, 10 ppm hydrogen) was measured as a function of the a/W ratio on an MTS servohydraulic fatigue testing machine at a stroke rate of 0.05 mm/s. Different a/W ratios were obtained by varying the depth of the saw-cut notch. The compliance data (i.e., the deflection per unit load C_s) are shown in a non-dimensional plot of EBC_s versus a/W in Fig. 5, where E is Young's modulus

*Calibration specimens were purchased from Effects Technology, Santa Barbara, CA.

and B is the specimen thickness. Ideally, a compliance calibration curve should be obtained with precracked specimens. However, as mentioned previously, difficulties were encountered in the preparation of precracked specimens of oxidized and homogenized material. The absence of a precrack and plane-strain conditions in the as-received material leads to somewhat higher values of EBC_S for a given a/W ratio compared to curves based upon thick, precracked specimens of other materials.[18] Since oxygen concentration and temperature over the ranges of 0.14 to 1.0 w % and 300 to 600 K, respectively, do not have a large effect on Young's modulus,[19] the curve in Fig. 5 will not result in additional uncertainty for Zircaloy specimens with oxygen concentrations of ≤1.0 wt %. The results in Fig. 5 were used to (a) determine the proper deflection for producing fatigue precracks in the three-point-bend rotary precracker and (b) calculate the corrected equivalent load in the case of elastic-plastic deformation, which is described in Section II.F. In the latter case, the curve in Fig. 5 can lead to an overestimate of the dynamic fracture toughness.

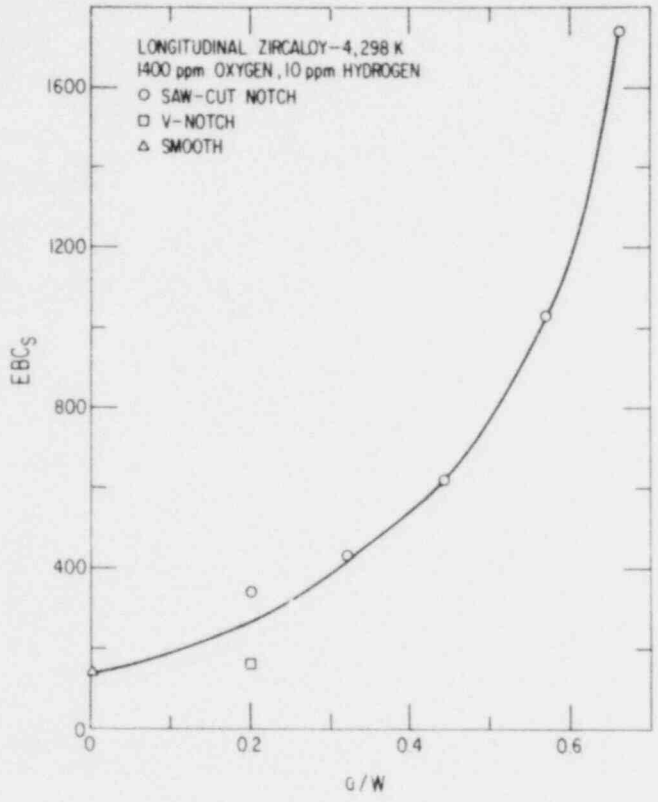

Fig. 5. Nondimensional Plot of the Compliance C_S of Zircaloy-4 Subsize Charpy Specimens at 298 K as a Function of the Crack Length to Specimen Width Ratio (a/W), Where E and B Are Young's Modulus and the Specimen Thickness, Respectively. ANL Neg. No. 306-7.

The impact test procedure was as follows: The specimen dimensions were measured and a macrophotograph of the notch area was obtained to provide a record of the transformed β-grain orientation near the root of the notch or tip of the precrack. A 0.25-mm-diameter Type K Chromel-Alumel thermocouple was spot welded near the specimen notch, ~1 mm away from notch root or crack tip. The dynamic response module, energy display module, and tup were calibrated, and with the specimen in place on the anvil and the striking tup held stationary at ~0.75 mm above the specimen, the fiber optic assembly was adjusted to ensure proper triggering of the oscilloscope, digital velocimeter display, and high-speed computerized data-acquisition system.

The specimen was properly positioned and centered on the anvils and the pneumatic valves were actuated to provide electrical contact between the specimen and the anvils. The sweep speed for the oscilloscope trace was set along with the optimum load and energy scale ranges and the storage facilities on the oscilloscope were cleared and reset. The floppy disk containing

the impact-data acquisition program was loaded on the Data General Nova II Computer System and the system was cleared and reset. The digital velocimeter-display module was also cleared and reset. The pneumatic system for the drop-tower actuation was switched on and the power supply was set to the desired voltage-current range. The temperature set point was positioned at the desired value and the temperature was monitored on the digital thermometer. When the test temperature was attained, the pneumatic specimen clamps were deactivated by the toggle switch on the control console. The cross-head drop switch was activated (which disconnected power to the specimen) and the impact event occurred. The oscilloscope traces (load-time and energy-time traces) were photographed. The velocimeter values were recorded and a preliminary load-time trace from the Nova-II computer data was obtained from an X-Y plotter. The preliminary trace was expanded on 250 mm x 380 mm graph paper by the X-Y plotter and the area under the curve was measured by polar planimeter.

E. Microstructural Evaluations

Optical and scanning-electron microscopy (SEM) were used to characterize the microstructure and fracture surface of the specimens. Polished specimens were etched in a solution of 50% distilled H_2O:45% HNO_3: 5% HF to reveal the grain structure. Anodization[20] of the specimens in a solution containing 0.06 m^3 absolute ethanol:0.035 m^3 H_2O:0.02 m^3 glycerine:0.01 m^3 lactic acid (85%):0.005 m^3 phosphoric acid (85%):0.02 kg citric acid was also used with polarized-light optics to obtain optimum contrast.

F. Impact Data Analysis

Figures 6 and 7 are load-versus-time traces for a homogeneous Zircaloy-oxygen alloy (0.63 wt % oxygen) and an as-received specimen with

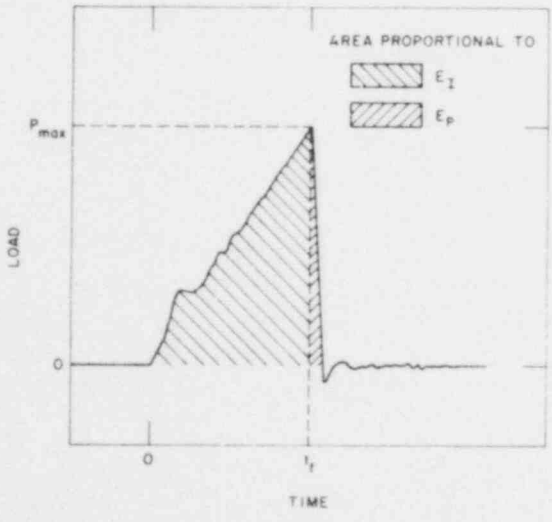

Fig. 6. Load-vs-Time Record for a Typical Linear-elastic Type Fracture of a Zircaloy-4 Specimen with 0.63 wt % Oxygen at 298 K. ANL Neg. No. 306-77-651.

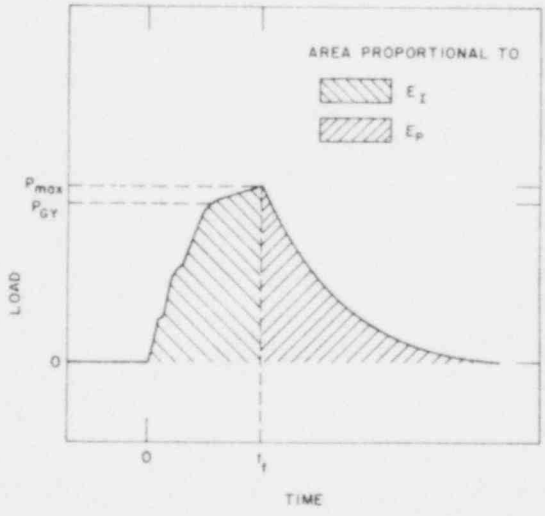

Fig. 7. Load-vs-Time Record for a Typical Elastic-plastic Type Fracture of an As-received Zircaloy-4 Specimen (0.14 wt % Oxygen) at 296 K. ANL Neg. No. 306-77-653.

0.14 wt % oxygen. The curve in Fig. 6 is typical of linear-elastic fracture, in which fracture occurs before measurable yielding of the specimen. In the as-received specimen (Fig. 7), yielding precedes an elastic-plastic fracture of the material. The load oscillations in the initial linear (elastic) portions of both curves are due to inertial effects.[21,22] The interference imposed by these oscillations during loading can be minimized by decreasing the initial impact velocity.

In Fig. 7, P_{GY} is the load at which general section yielding occurs. If fracture (i.e., unstable propagation of a crack) is assumed to initiate at the maximum load P_{max}, the area under the load-time trace, which is directly related to the total energy ΔE_0 absorbed by the specimen, can be divided into two parts: the energy required for fracture initiation E_I (energy for crack initiation and crack stable propagation) and that for propagation E_P (energy for unstable crack propagation). Both energy values can be normalized with respect to the fracture area, and a ductility index[23,24] can be defined as

$$D_I = \frac{E_P}{E_I}. \tag{1}$$

The dynamic fracture toughness K_{ID} can be calculated from Eq. 2 for specimens that exhibit linear-elastic behavior, in which fracture occurs before general yielding (i.e., $P_{max} < P_{GY}$ in Fig. 6):

$$K_{ID} = \frac{6Ya^{0.5}P_{max}}{BW^{1.5}}, \tag{2}$$

where Y is a function of a/W and can be obtained from reported curves.[15]

For specimens that exhibit elastic-plastic deformation before fracture ($P_{max} > P_{GY}$), the fracture toughness can be calculated by the equivalent-energy method. The analysis requires E_I, the corrected energy to initiate fracture, which can be obtained from

$$E_I = W_I - E_m, \tag{3}$$

where W_I represents the energy associated with the maximum load on the load-time record, and E_m is the elastic stored energy in the testing machine, which can be obtained from the machine compliance C_m. The machine compliance can be represented by

$$C_m = C_t - C_s, \tag{4}$$

where C_t and C_s are the total system and specimen compliances, respectively. The specimen compliance can be obtained from a plot of EBC_s versus the ratio of the specimen notch depth to width a/W, where E is the elastic modulus of the specimen material and B is the specimen thickness (Fig. 5). The

total compliance can be obtained from the elastic portion of the load-time trace; i.e.,

$$C_t = D_a/P_a, \tag{5}$$

where D_a is the apparent combined deflection of the specimen and the machine under the load P_a. The deflection D_a can be obtained from

$$D_a = \bar{v}t_a, \tag{6}$$

where $\bar{v}$ is the average velocity of the crosshead during impact, and t_a is the time to produce fracture in the specimen. The elastic stored energy in the machine can be obtained from

$$E_m = \frac{P_{max}^2 C_m}{2}, \tag{7}$$

and the result can be substituted into Eq. 3 to obtain values for E_I. The equivalent load P^* is given by

$$P^* = \frac{2E_I^{0.5}}{C_s}. \tag{8}$$

The equivalent-energy fracture toughness K_D^* can be calculated by substituting the value of P^* into Eq. 2.

The uncertainties associated with the various measured and calculated quantities are discussed in Appendix A.

III. RESULTS

A. Impact Properties of Zircaloy-Oxygen Alloys

The influence of oxygen concentration and temperature on the maximum load, energies for crack initiation and propagation, total absorbed energy, dynamic fracture toughness, ductility index, and fracture mode of Zircaloy-2 and -4 specimens has been evaluated from the impact-test results. The effect of oxygen concentration on the maximum load for notched and precracked specimens of Zircaloy-2 and -4 with longitudinal and transverse textures is shown in Fig. 8 for temperatures of 373, 473, 623, and 823 K. At temperatures between 373 and 673 K and for oxygen concentrations of ≤1.0 wt %, higher loads

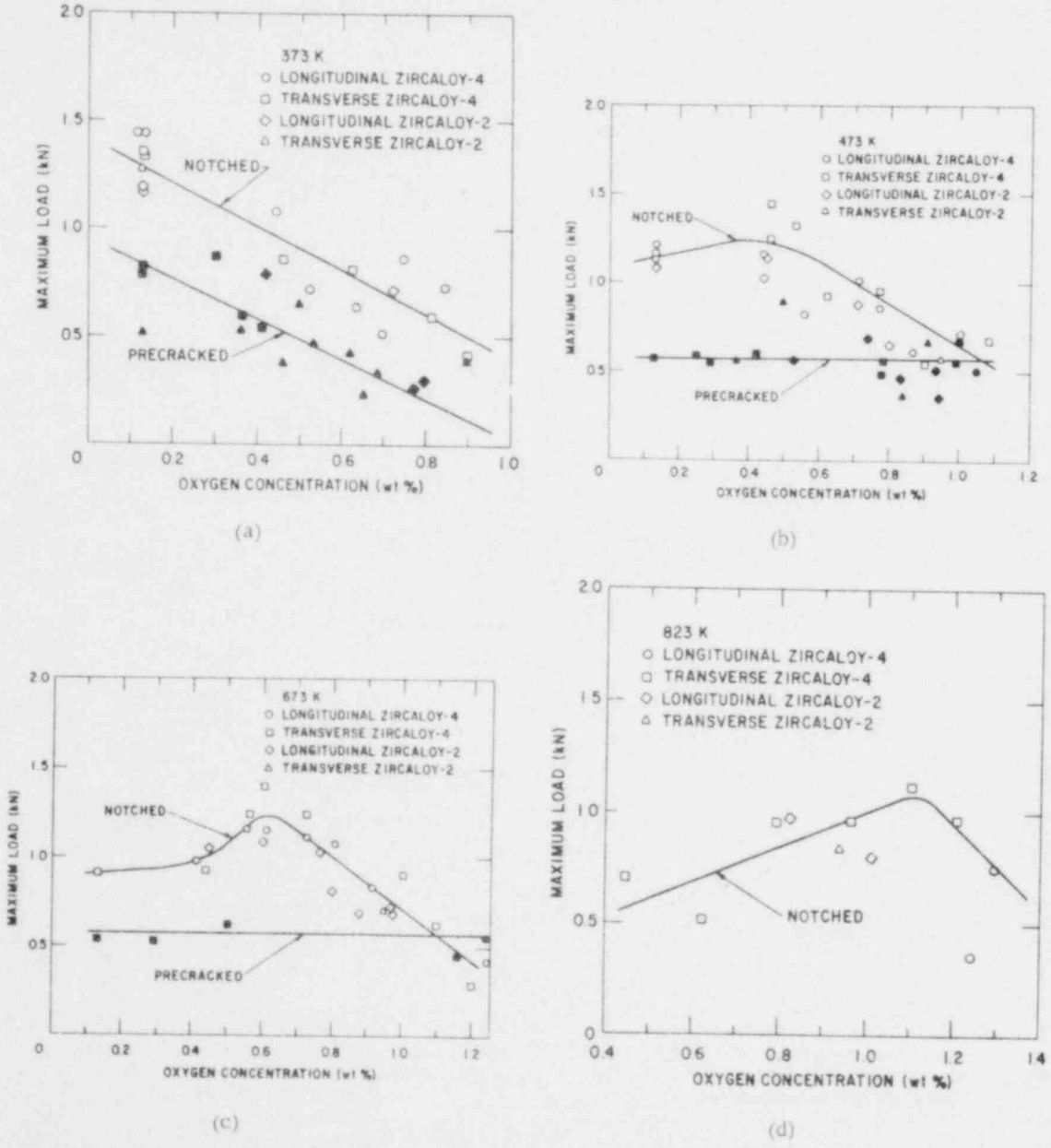

Fig. 8. Effect of Oxygen Concentration on Maximum Load for Notched and Precracked Zircaloy-2 and -4 Specimens with Longitudinal and Transverse Textures at Temperatures of (a) 373, (b) 473, (c) 673, and (d) 823 K. Impact velocity was 0.75 m/s. Neg. Nos. MSD-65987, -65970, -65992 and -65971.

are required for crack initiation in notched specimens than for precracked specimens. Texture (i.e., specimen orientation with respect to the rolling direction of the plate) and material (i.e., Zircaloy-2 or -4) have no effect on the maximum load within the uncertainty of the experimental results.

Figure 9 shows the temperature dependence of the maximum load for homogeneous Zircaloy-oxygen alloys with several oxygen concentrations

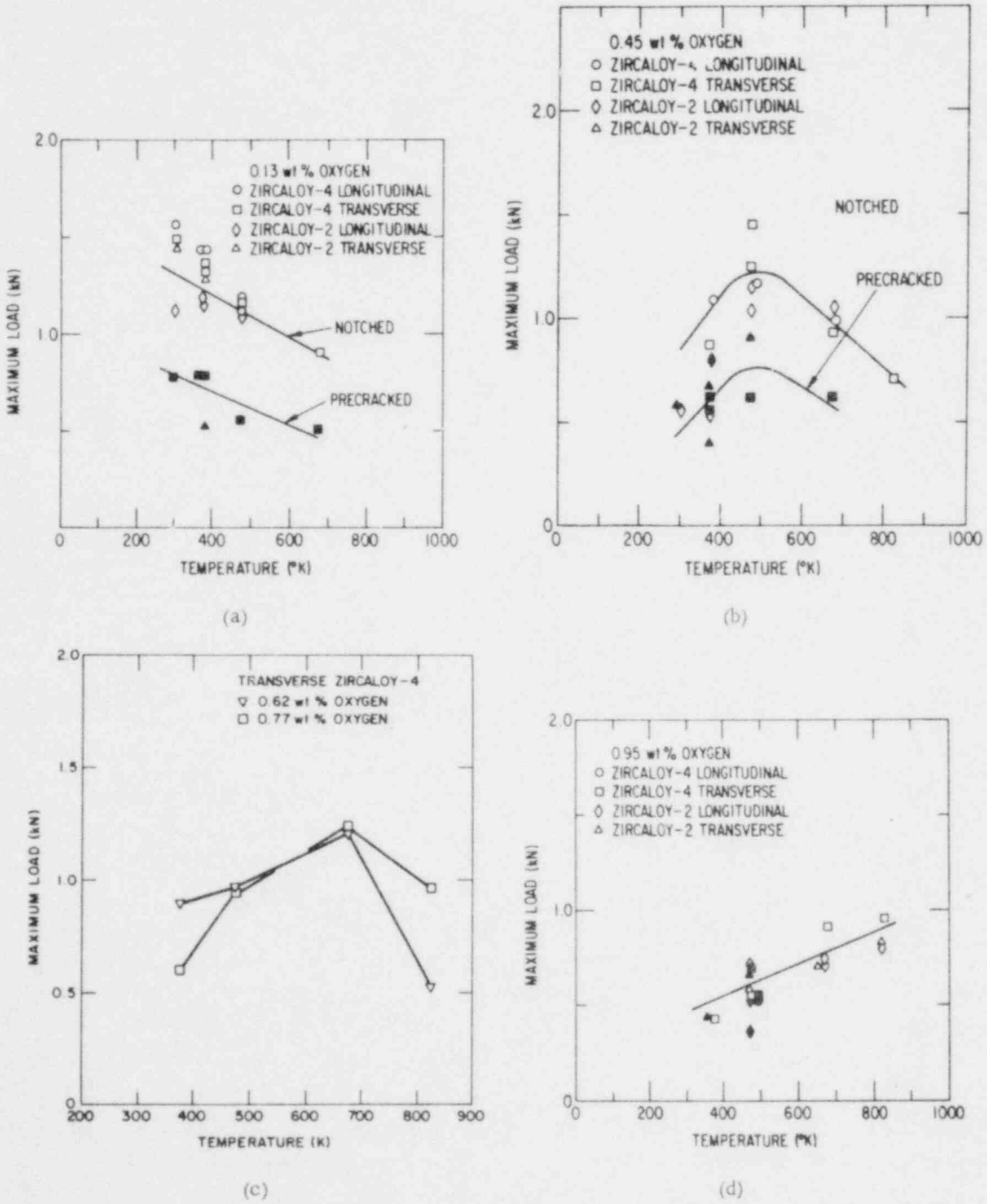

Fig. 9. Effect of Temperature on Maximum Load for Homogeneous Zircaloy-Oxygen Alloys with (a) 0.13, (b) 0.45, (c) 0.62 and 0.77, and (d) 0.95 wt % Oxygen. Open and closed symbols refer to notched and fatigue-precracked specimens, respectively. Impact velocity was 0.75 m/s. Neg Nos. MSD-65987, -65928, -65160, and 65916.

between 0.13 and 0.95 wt %. For specimens that exhibit some degree of plastic deformation (i.e., the maximum load is greater than the yield load, Fig. 7) and a predominantly ductile fracture mode, the maximum load decreases as the temperature increases, e.g., as-received Zircaloy with 0.13 wt % oxygen (Fig. 9a). In contrast, the maximum load increases as the temperature increases for specimens that fracture in a brittle manner, e.g., material with 0.45, 0.62-0.7[illegible], and 0.95 wt % oxygen at temperatures below ~473, 673, and 823 K, respectively (Figs. 9b-d). The maxima in the load-versus-temperature curves at ~473 and 673 K in Figs. 9b and 9c indicate a transition from a predominantly brittle to ductile fracture mode as the temperature increases.

The effect of oxygen concentration on the crack initiation energy per area is shown in Fig. 10 for several temperatures between 373 and 823 K. The crack initiation energy, which is the absorbed energy to the point of maximum load in Figs. 6 and 7, represents the energy for stable propagation of a crack in precracked specimens and for initiation and stable propagation in notched specimens. The crack initiation energies decrease as the oxygen concentration increases at the various temperatures, and the values become independent of oxygen concentration, texture, and geometry (notch versus precrack) under conditions where predominantly brittle fracture occurs. The temperature dependence of the crack initiation energy for transverse Zircaloy-4 specimens with oxygen concentrations between 0.13 and 0.95 wt % is shown in Fig 11. At high oxygen concentrations (e.g., $\geq$0.75 wt % in Fig. 12), the crack initiation energy for notched and fatigue-precracked specimens is similar, and the type of material and texture have no effect on this parameter.

Figure 13 shows the dependence of the crack-propagation energy (i.e., the energy absorbed by the specimen after the point of maximum load on the load-versus-time curve) on oxygen concentration at 373, 473, and 673 K. The energy expended in unstable crack propagation is quite low ($\leq 1 \times 10^4$ J/m^2) for oxygen concentrations $\geq$0.5 wt % at 373 and 473 K. The effect of oxygen concentration in Zircaloy-2 and -4 on the total absorbed energy for notched and precracked specimens with longitudinal and transverse textures is shown in Fig. 14 for several temperatures between 373 and 823 K.

The ductility index, which is the ratio of the energy for unstable crack propagation to the energy for crack initiation and stable crack propagation (Eq. 1), is shown in Fig. 15. Because of the energy associated with crack initiation in notched specimens, the ductility index is lower than for precracked specimens.

Figure 16 shows the dynamic fracture toughness, calculated from Eq. 2, for Zircaloy-oxygen alloys at several temperatures between 373 and 823 K. The fracture toughness decreases rapidly to a value of ~10 MPa·m$^{1/2}$ as the oxygen concentration increases, and the curves shift in the direction of higher oxygen concentration as the temperature increases. The effect of temperature on the fracture toughness of Zircaloy containing 0.45 and 0.95 wt % oxygen is depicted in Fig. 17. For oxygen concentrations between ~0.45 and 0.95 wt %, the temperature dependence of the fracture toughness over the range of ~300 to 700 K is small.

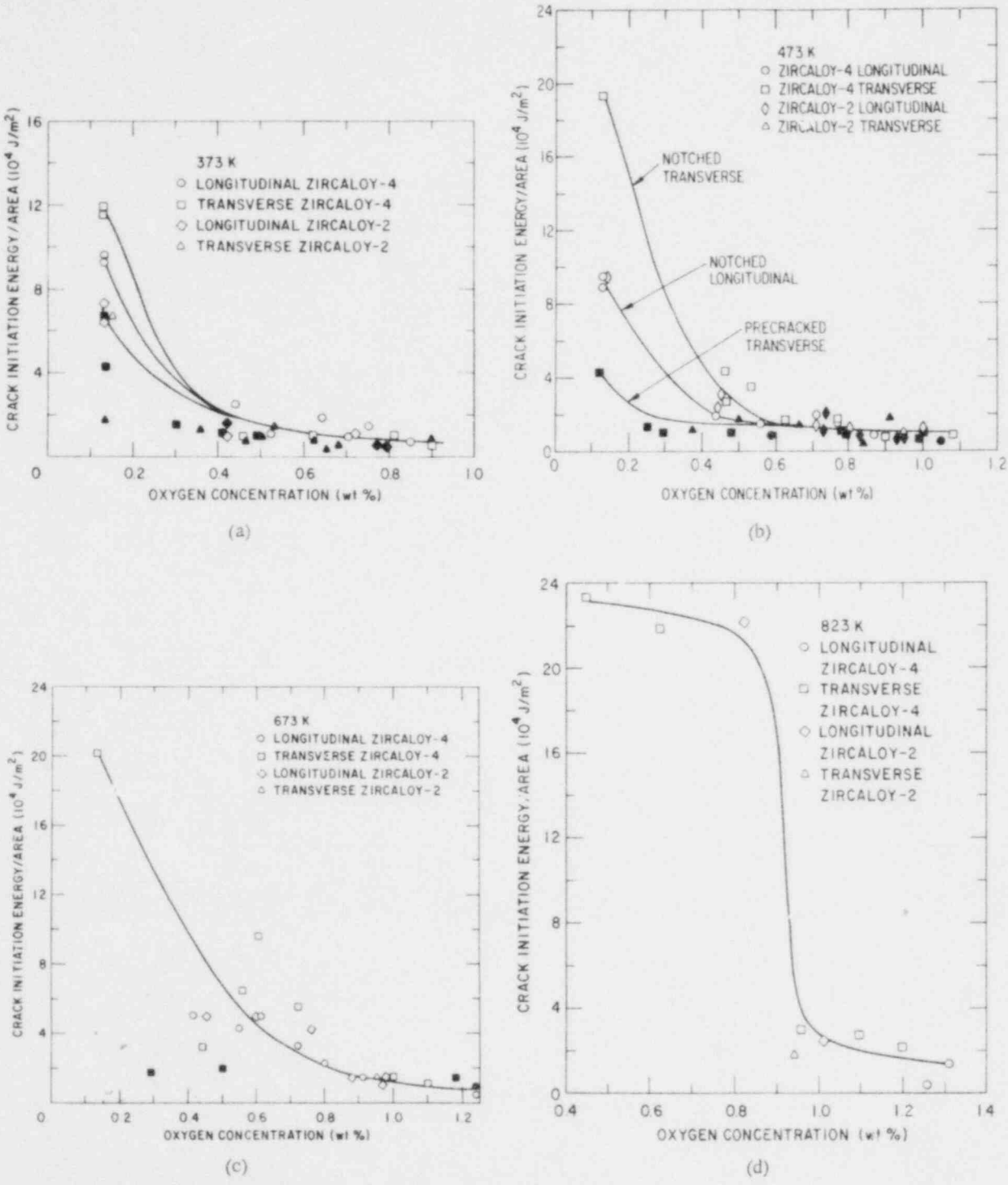

Fig. 10. Effect of Oxygen Concentration on Crack Initiation Energy per Unit Area for Homogeneous Zircaloy-2 and -4 Specimens with Longitudinal and Transverse Textures at Temperatures of (a) 373, (b) 473, (c) 673, and (d) 823 K. Open and closed symbols refer to notched and fatigue-precracked specimens, respectively. Impact velocity was 0.75 m/s. Neg. Nos. MSD-65990, -65915, -65991, and -65989.

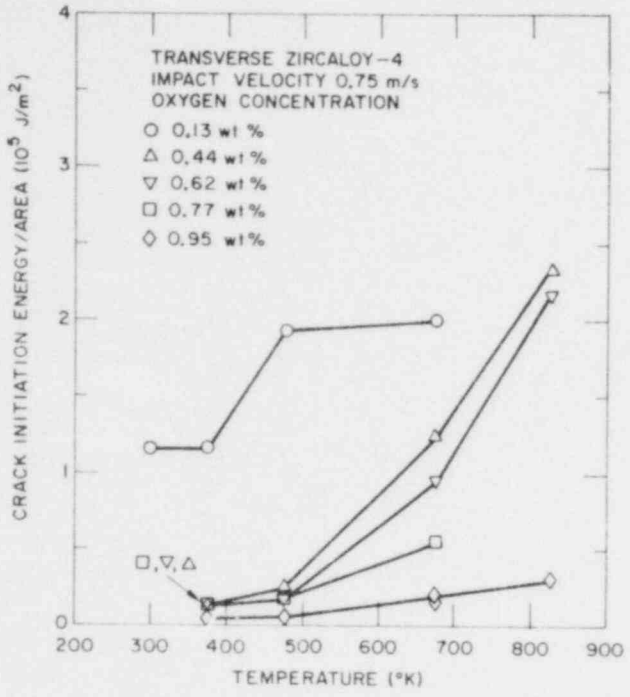

Fig. 11

Effect of Temperature on Crack Initiation Energy per Unit Area for Transverse Zircaloy-4 Specimens with Oxygen Concentrations between 0.13 and 0.95 wt %. Neg. No. MSD-65161.

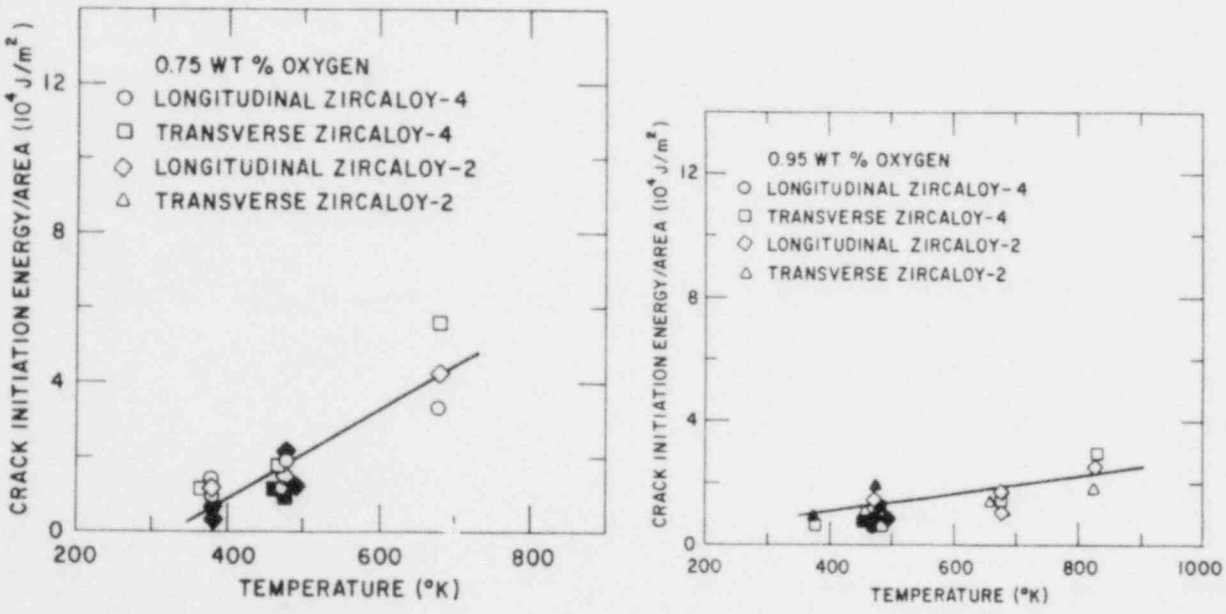

Fig. 12. Dependence of Crack Initiation Energy per Unit Area on Temperature for Homogeneous Zircaloy-2 and -4 Specimens with (a) 0.75 and (b) 0.95 wt % Oxygen. Open and closed symbols refer to notched and fatigue-precracked specimens, respectively. Impact velocity was 0.75 m/s. Neg. Nos. MSD-65988 and -65983.

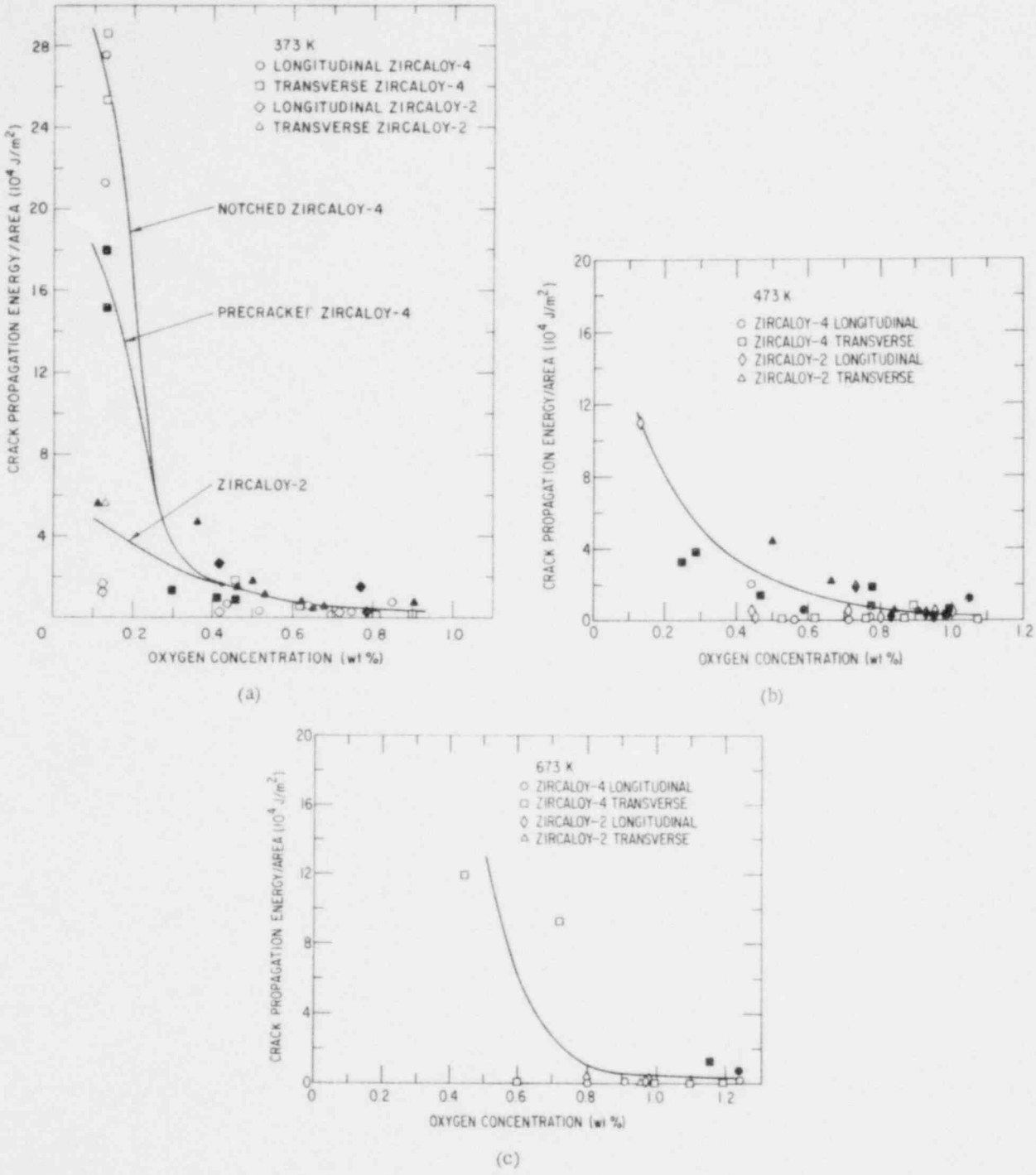

Fig. 13. Effect of Oxygen Concentration on Crack Propagation Energy per Unit Area of Homogeneous Zircaloy-2 and -4 Specimens with Longitudinal and Transverse Textures at Temperatures of (a) 373, (b) 473, and (c) 673 K. Open and closed symbols refer to notched and fatigue-precracked specimens, respectively. Impact velocity was 0.75 m/s. Neg. Nos. MSD-65975, -65924, and -65921.

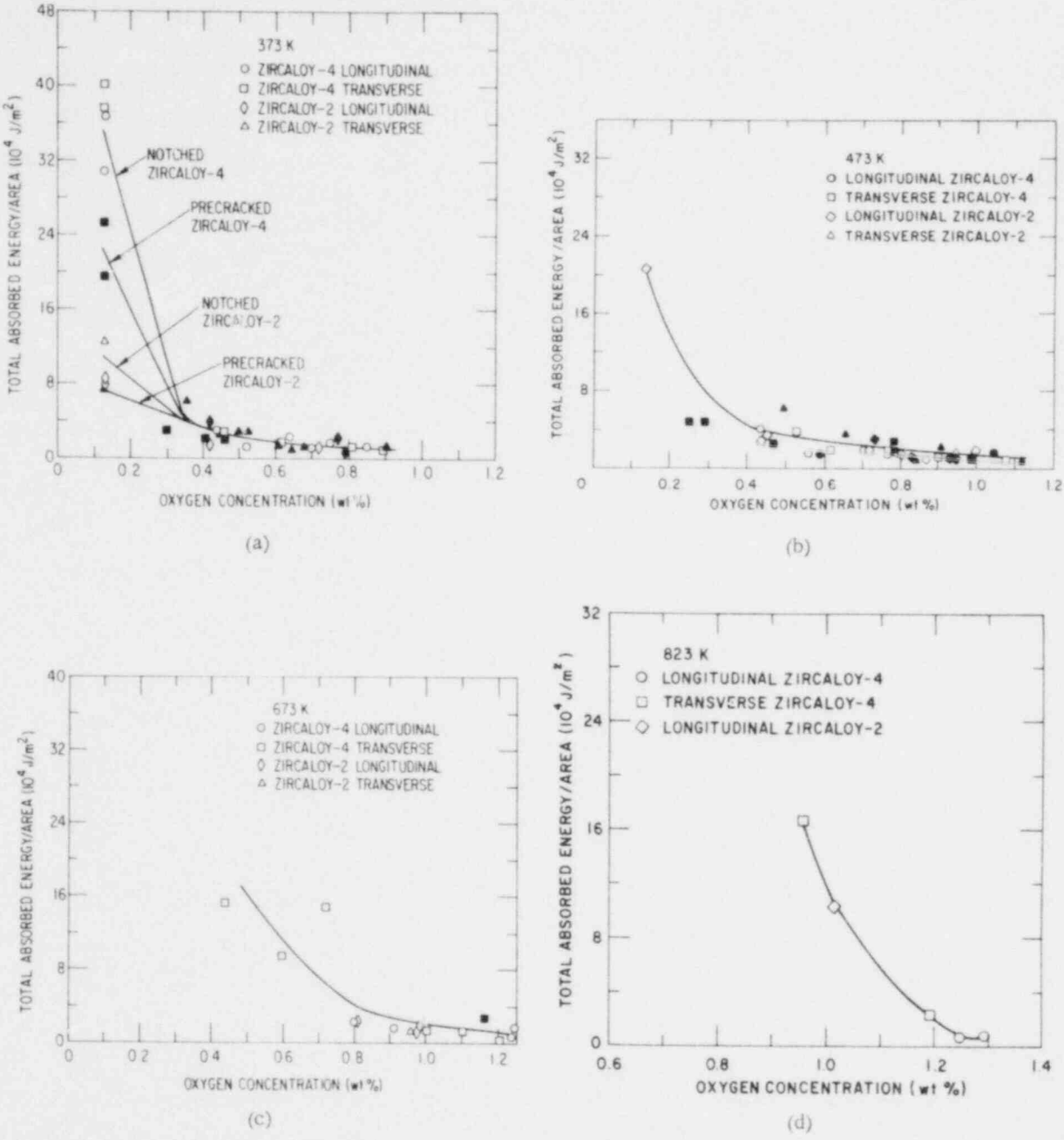

Fig. 14. Total Absorbed Energy per Unit Area as a Function of Oxygen Concentration of Homogeneous Zircaloy-2 and -4 Specimens with Longitudinal and Transverse Textures at Temperatures of (a) 373, (b) 473, (c) 673, and (d) 823 K. Open and closed symbols refer to notched and fatigue-precracked specimens, respectively. Impact velocity was 0.75 m/s. Neg. Nos. MSD-65917, -65980, -65926, and -65974.

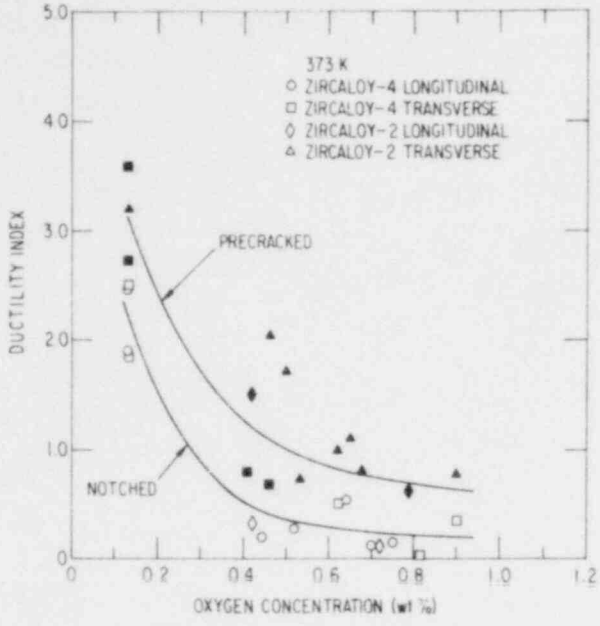

(a)

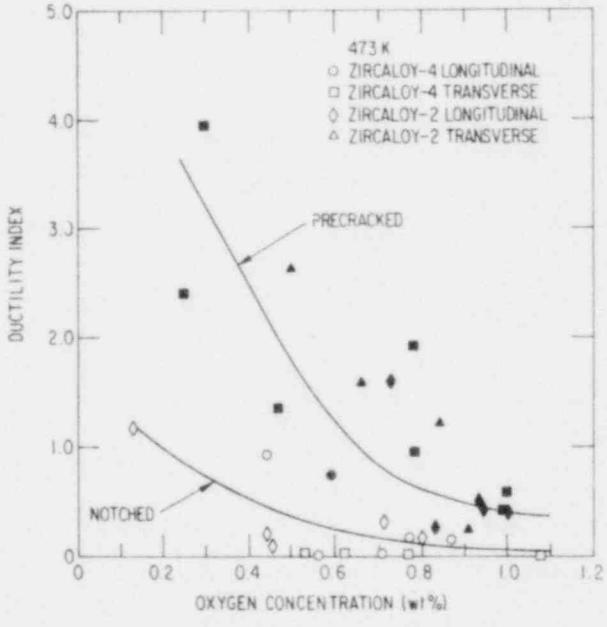

(b)

Fig. 15. Ductility Index as a Function of Oxygen Concentration of Homogeneous Zircaloy-2 and -4 Specimens at Temperatures of (a) 373 and (b) 473 K. Open and closed symbols refer to notched and fatigue-precracked specimens, respectively. Impact velocity was 0.75 m/s. Neg. Nos. MSD-65918 and -65920.

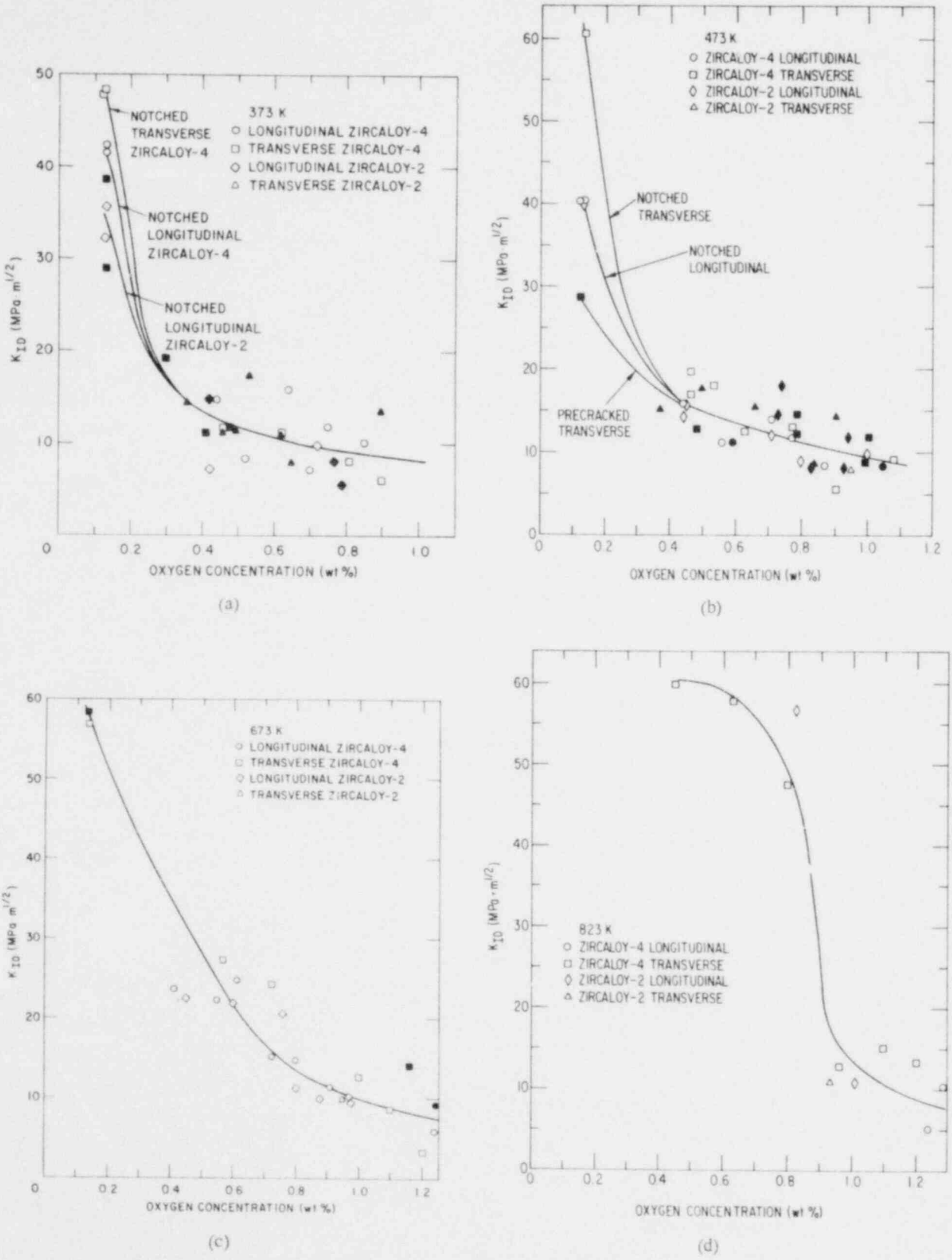

Fig. 16. Dynamic Fracture Toughness as a Function of Oxygen Concentration of Homogeneous Zircaloy-2 and -4 Specimens with Longitudinal and Transverse Textures at Temperatures of (a) 373, (b) 473, (c) 673, and (d) 823 K. Open and closed symbols refer to notched and fatigue-precracked specimens, respectively. Impact velocity was 0.75 m/s. Neg. Nos. MSD-65968, -65923, 65984, and -65922.

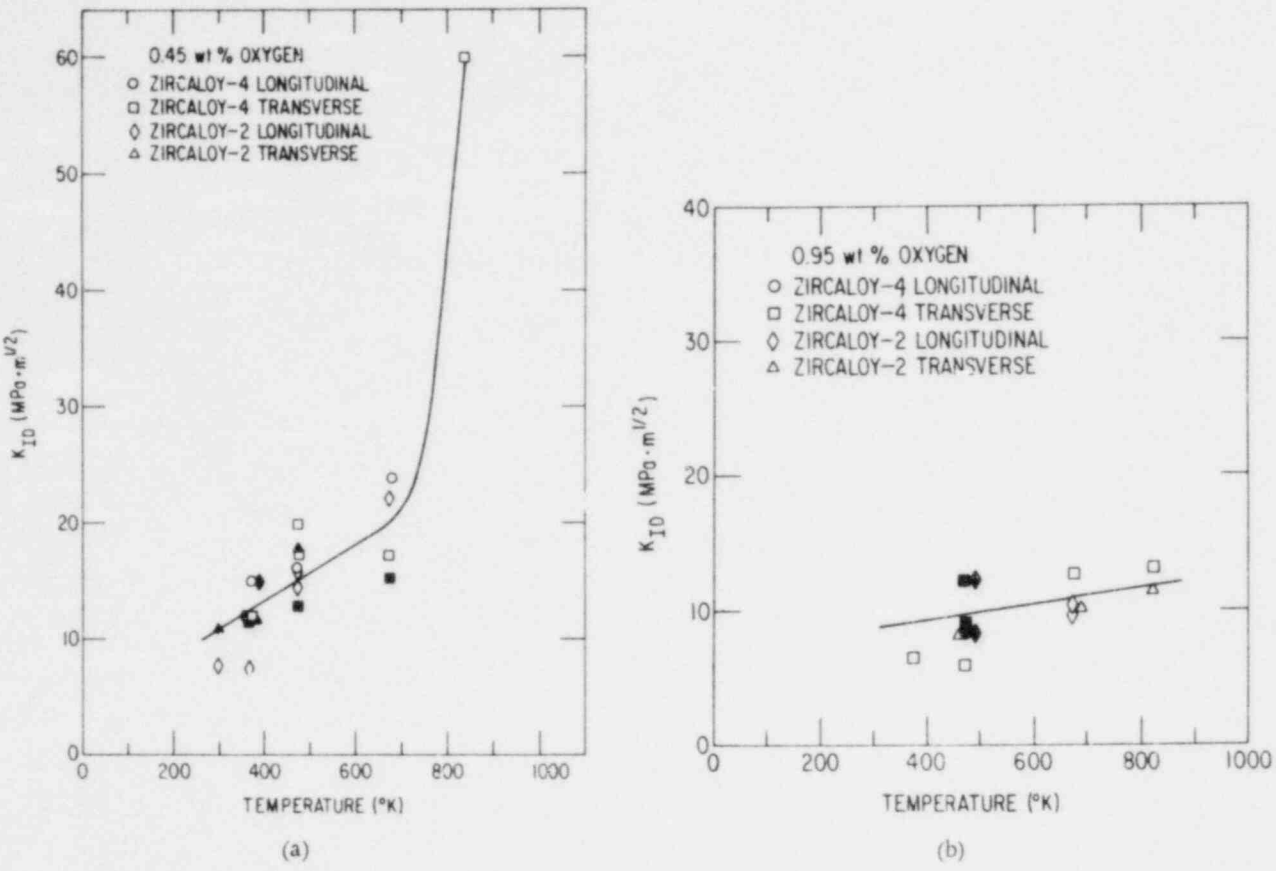

Fig. 17. Effect of Temperature on Dynamic Fracture Toughness of Homogeneous Zircaloy-2 and -4 Specimens Containing (a) 0.45 and (b) 0.95 wt % Oxygen. Open and closed symbols refer to notched and fatigue-precracked specimens, respectively. Impact velocity was 0.75 m/s. Neg. Nos. MSD-65925 and -54919.

The fracture surfaces of the impact specimens were examined by SEM to evaluate the fracture mode as functions of temperature and oxygen concentration of the material. Figure 18 shows the fracture surfaces of Zircaloy specimens with 0.75 wt % oxygen that were impact-tested at four temperatures between 373 and 823 K. As the test temperature increases, the fraction of the cross sectional area that exhibits ductile failure increases. For example, in Fig. 18a, the high-oxygen α' platelets fail in a brittle manner, as evidenced by the "river patterns," whereas the oxygen-depleted regions exhibit a dimpled appearance characteristic of ductile fracture. The relative surface area of the dimpled region increases in Fig. 18b; however, fracture occurred in a predominantly brittle manner. At higher temperatures (Figs. 18c and 18d), the dimpled surfaces are characteristic of fully ductile fracture. Figure 19 shows other examples of predominantly brittle fracture in specimens with 0.62 and 1.10 wt % oxygen that were tested at 373 and 473 K, respectively.

The impact-property results, which were presented graphically in Figs. 14-17 and are tabulated in Appendix B, can be used to develop a set of self-consistent criteria for the transition from ductile to brittle fracture relative to the temperature and oxygen concentration in the material. Criteria based upon impact measurements, SEM evaluation of the fracture surfaces,

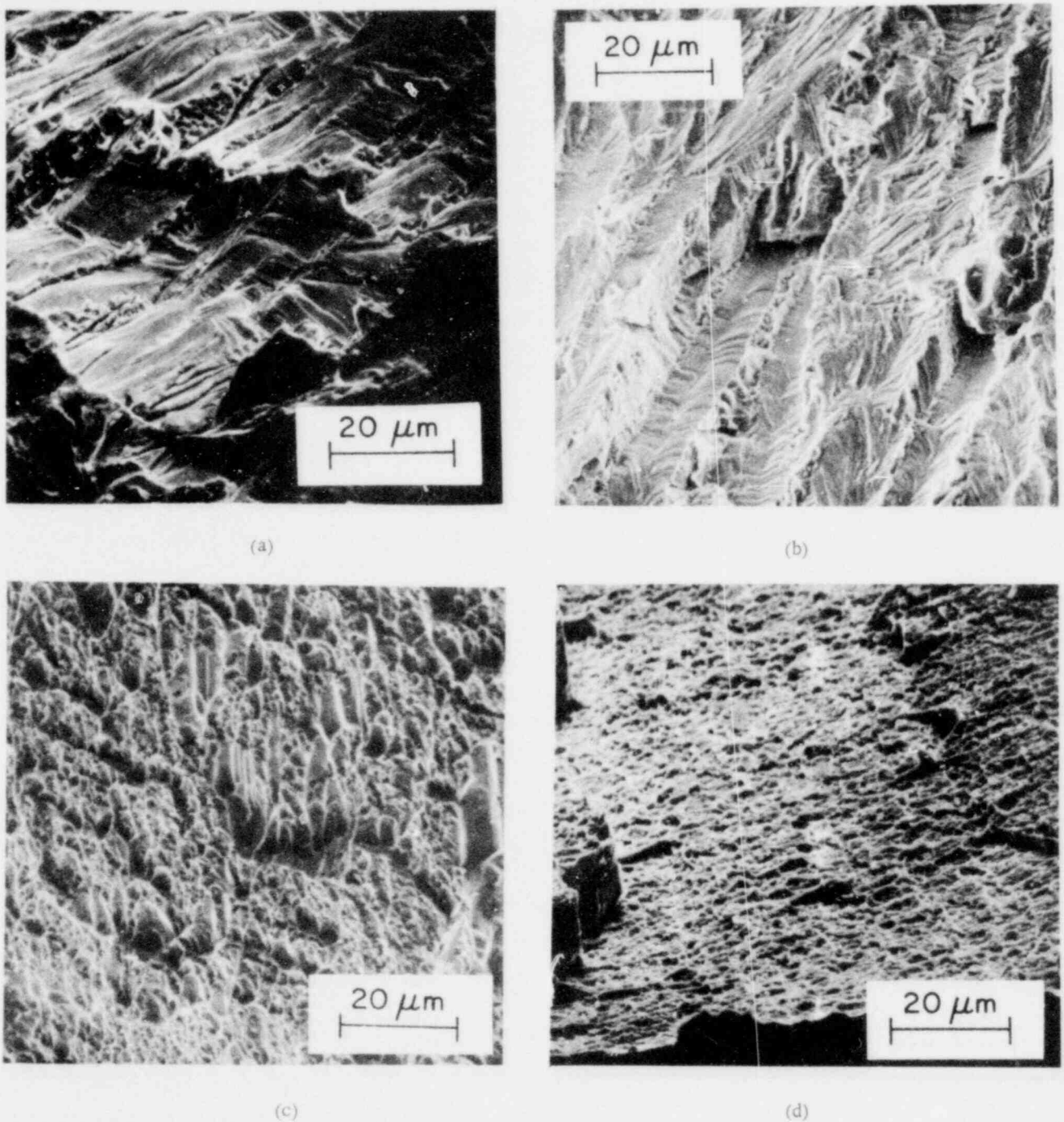

(a) (b)

(c) (d)

Fig. 18. SEM Fractographs of Homogeneous Zircaloy-4 Specimens with 0.75 wt % Oxygen Fractured at (a) 373, (b) 473, (c) 673, and (d) 823 K. Brittle fracture of the high-oxygen α' plates is evident from the river patterns in (a) and (b), whereas the dimpled appearance in (c) and (d) is indicative of ductile fracture. Neg. Nos. MSD-65150, -65148, -65147, and -65146.

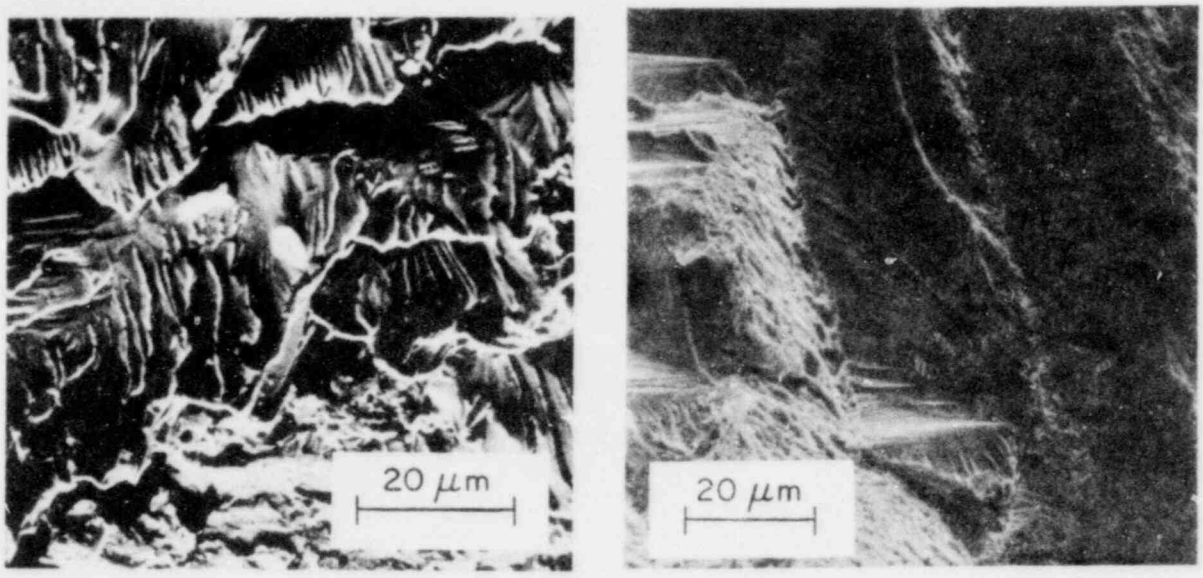

(a) (b)

Fig. 19. SEM Fractographs of Homogeneous Zircaloy-4 Specimens with (a) 0.62 and (b) 1.10 wt % Oxygen Fractured at 373 and 473 K, Respectively. Fracture occurred in a predominantly brittle manner at both temperatures. Neg. Nos. MSD-65149 and -54145.

and deflection angle of the fractured specimens are shown in Fig. 20. For conditions of temperature and oxygen to the right of the lines in Figs. 20a and 20b, fracture will occur at a total absorbed energy of ~1.3×10^4 J/m^2 and the material will have a dynamic toughness of ~10 MPa·m$^{1/2}$, respectively. In Fig. 20c, conditions of temperature and oxygen concentration to the left of the line correspond to a ductility index of >0. These criteria are consistent with the boundaries in Figs. 20d and 20e, which are based upon a ductile area (dimple region) < 25% of the fracture surface and a deflection angle of < 5°, respectively. Specimens with high ductility exhibited deflection angles of ~90° and cleared the gap between the anvils of the impact machine, but did not fracture.

B. Impact Properties of Zircaloy-Hydrogen Alloys

Hydrogen uptake by Zircaloy fuel cladding occurs after rupture under internal pressure and high-temperature oxidation in steam.[5] Consequently, the influence of hydrogen as well as oxygen on the impact properties of Zircaloy is of interest in an analysis of the response of fuel cladding to mechanical loads at low temperatures.

The maximum load during impact of notched Zircaloy-2 specimens is virtually independent of hydrogen content and temperature over the ranges of 600 to 1400 wt ppm and 373 to 673 K, respectively, within the uncertainty of the load values in Fig. 21. Since the terminal solubility of hydrogen in Zircaloy is ~200 wt ppm at 673 K and the concentration decreases with temperature,[25-27]

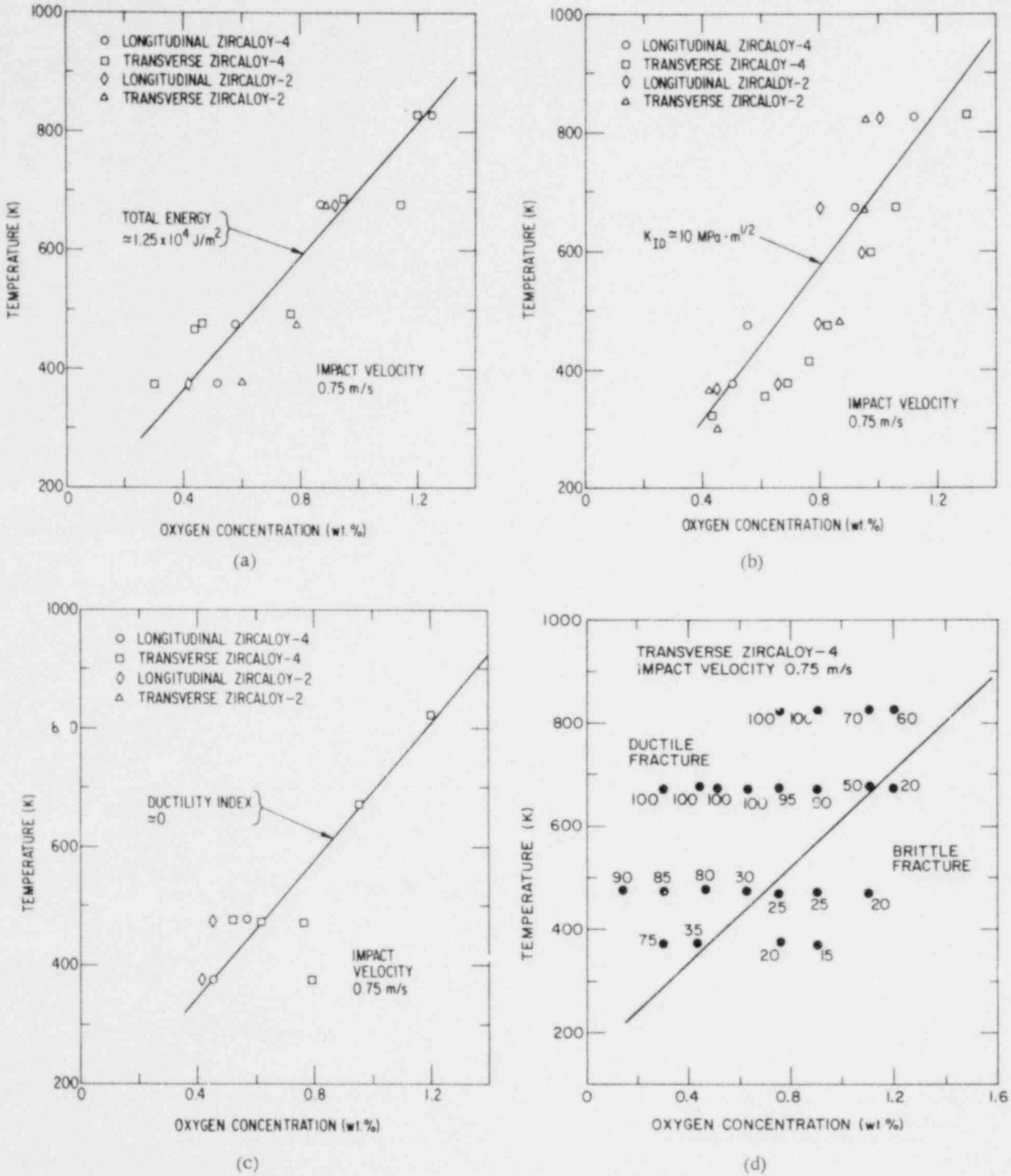

Fig. 20. Ductile-to-brittle Transition as a Function of Temperature and Oxygen Concentration of Homogeneous Zircaloy-2 and -4 Alloys Based Upon the Following Criteria: (a) Total Absorbed Energy of ~1.3 x 10^4 J/m^2, (b) Dynamic Fracture Toughness of ~10 MPa·$m^{1/2}$, (c) Ductility Index of ~0, (d) <25% of the Fracture Surface Area Exhibiting Shear Dimples, and (e) Deflection Angle of the Deformed Specimens of <5°

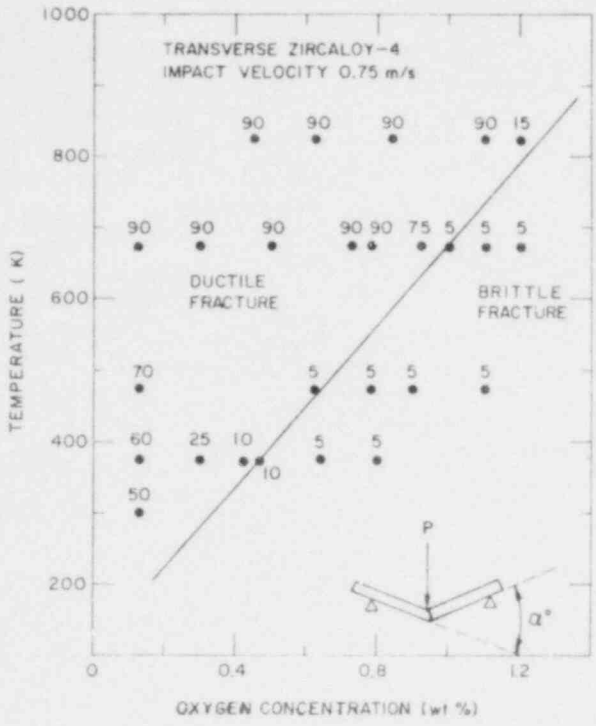

(c)

Fig. 20 (Contd.)

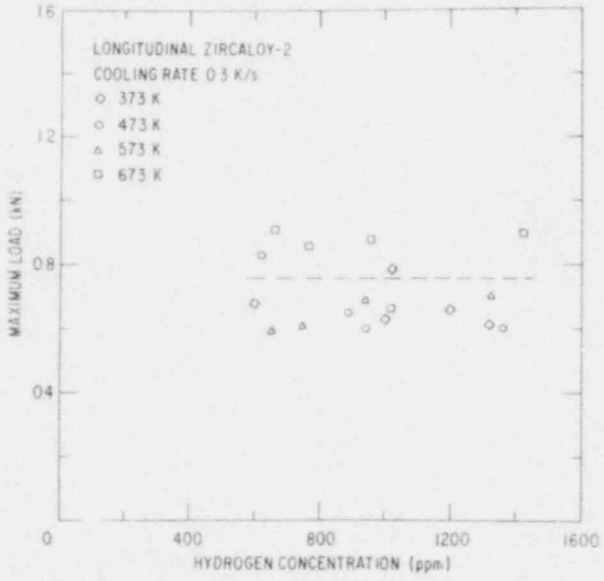

Fig. 21

Maximum Load as a Function of Hydrogen Concentration of Zircaloy-2 Specimens with Longitudinal Texture at Several Temperatures between 373 and 673 K. Specimens were cooled through the temperature range of the $\beta \rightarrow \alpha' +$ hydride phase transformation at a rate of ~0.3 K/s.

the hydride phase is present in the material for the range of conditions in this investigation. The influence of hydrogen concentration on the crack initiation energy for longitudinal Zircaloy-2 specimens, which were cooled through the temperature range of the $\beta \rightarrow \alpha' +$ hydride phase transformation at rates of ~3 and 0.3 K/s, is shown in Fig. 22 for several temperatures between 373 and 673 K. The crack initiation energy for specimens cooled through the phase transformation at a rate of ~0.3 K/s is independent of hydrogen concentration ($\geq$600 wt ppm) for temperatures $\leq$573 K (Fig. 22b). Both temperature and hydrogen content have a strong influence on the crack initiation energy of impact specimens that were cooled through the phase transformation at the higher rate (Fig. 22a).

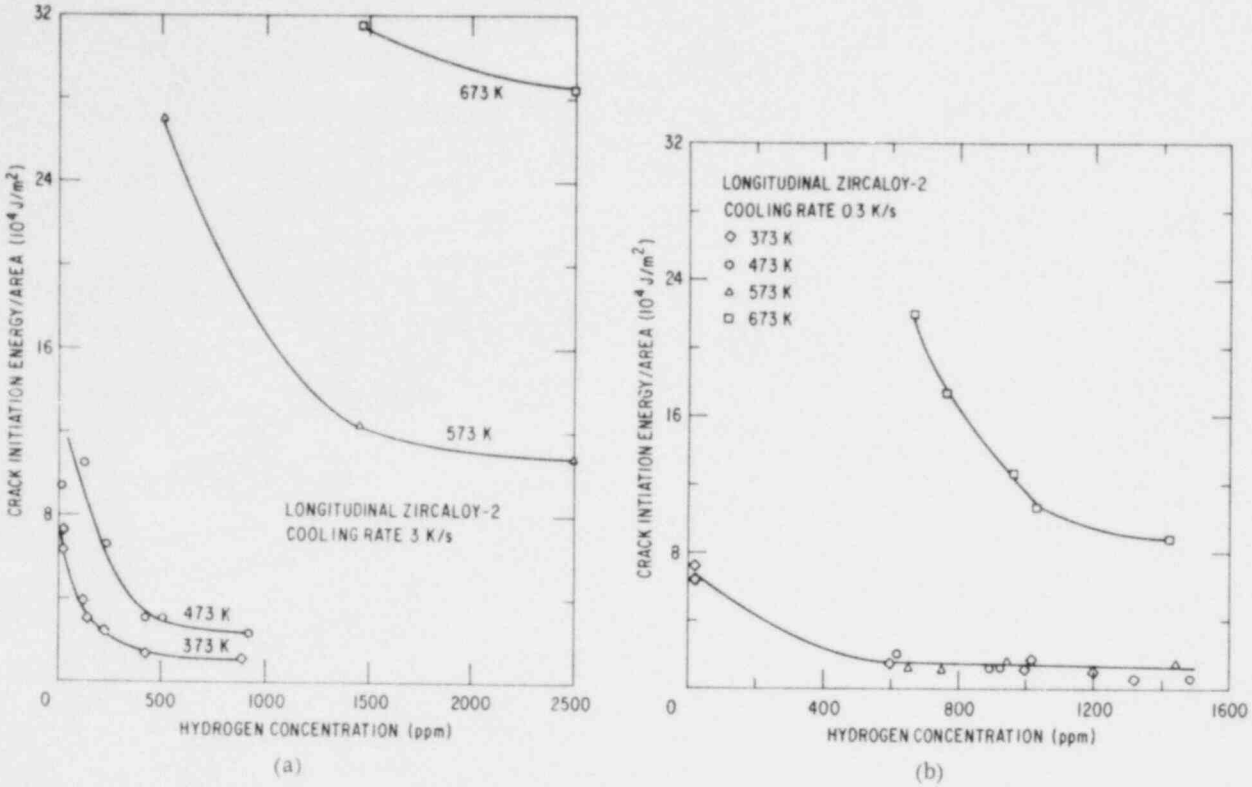

Fig. 22. Crack Initiation Energy per Unit Area as a Function of Hydrogen Concentration in Zircaloy-2 Specimens at Several Temperatures between 373 and 673 K. The subsize Charpy specimens with longitudinal texture were cooled through the temperature range of the $\beta \rightarrow \alpha' +$ hydride phase transformation at rates of (a) 3 K/s and (b) 0.3 K/s. Neg. Nos. MSD-66183 and -66177.

The dependence of the crack propagation energy on hydrogen concentration for specimens that were charged with hydrogen and cooled through the temperature range of the phase transformation at rates of ~3 and 0.3 K/s is shown in Fig. 23. At 373 and 473 K, the fracture propagation energies for materials with equivalent hydrogen contents ($\geq$400 wt ppm) at the two cooling rates are similar ($\leq 3 \times 10^4$ J/m^2). The results in Figs. 22 and 23 show that at 373 K, the crack initiation energy is a strong function of the hydrogen content over the range of ~10 to 600 wt ppm, whereas the crack propagation energy is relatively independent of hydrogen concentration. These data are consistent with Westlake's observation that hydrides promote crack initiation but crack propagation is controlled by the ductility of the zirconium matrix at low temperatures (77 K).[28] Hardie indicates that the crack propagation characteristics are determined by the interhydride spacing and the flow properties of the matrix.[29]

The effect of hydrogen on the total absorbed energy of the Zircaloy-2 specimens is shown in Fig. 24. These results are in qualitative agreement with absorbed energy data for a Zr-2.5 wt % Nb alloy[30] and cold-worked Zircaloy-2 (Ref. 31) with ~13 to 250 wt ppm hydrogen.

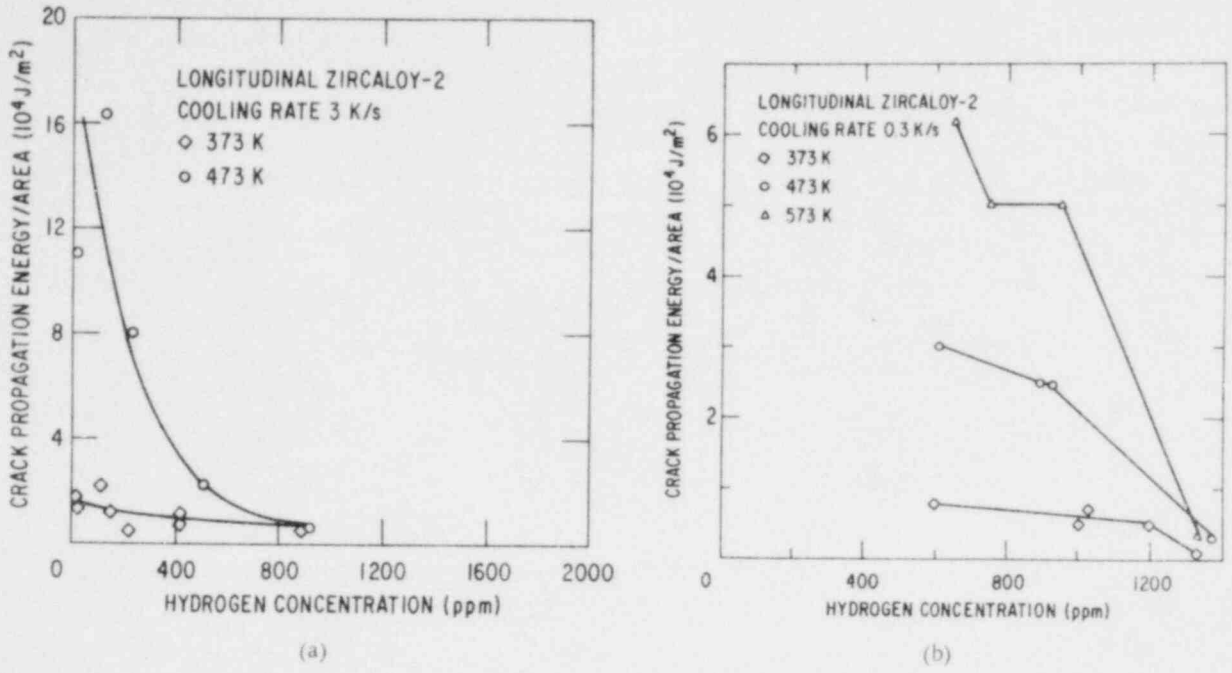

Fig. 23. Crack Propagation Energy per Unit Area as a Function of Hydrogen Concentration in Zircaloy-2 Specimens at Several Temperatures between 373 and 573 K. The subsize Charpy specimens with longitudinal texture were cooled through the temperature range of the $\beta \rightarrow \alpha' +$ hydride phase transformation at rates of (a) 3 K/s and (b) 0.3 K/s. Impact velocity was 0.75 m/s. Neg. Nos. MSD-66174 and -66176.

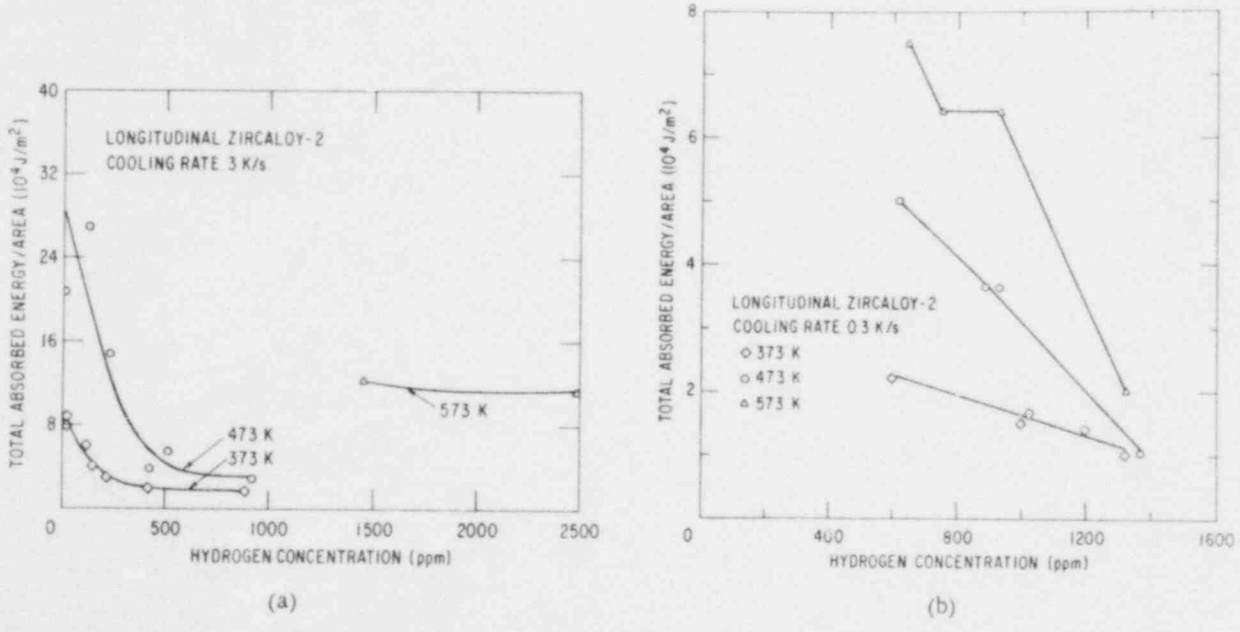

Fig. 24. Total Absorbed Energy per Unit Area as a Function of Hydrogen Concentration in Zircaloy-2 Specimens at Several Temperatures between 373 and 573 K. The subsize Charpy specimens with longitudinal texture were cooled through the temperature range of the $\beta \rightarrow \alpha' +$ hydride phase transformation at rates of (a) 3 K/s and (b) 0.3 K/s. Impact velocity was 0.75 m/s. Neg. Nos. MSD-66182 and -66181.

Figure 25 shows the dependence of the ductility index on hydrogen concentration at several temperatures. At 373 K, the ductility index is quite small (~0.5) and independent of the hydrogen content (≥600 wt ppm); however, at 573 K, the ductility index is large and decreases linearly with hydrogen concentration over the range of ~600 to 1300 wt ppm.

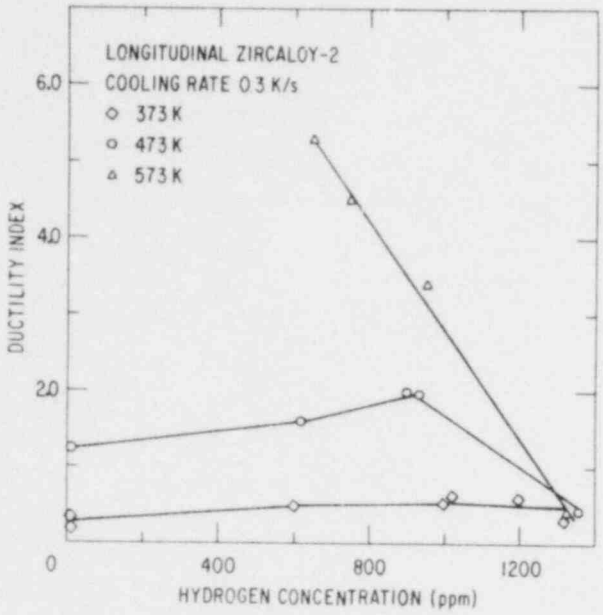

Fig. 25

Ductility Index of Zircaloy-2 Specimens as a Function of Hydrogen Concentration at Temperatures of 373, 473, and 573 K. Neg. No. MSD-66179.

The effect of hydrogen on the dynamic fracture toughness of Zircaloy-2 specimens, which were cooled through the temperature range of the $\beta \rightarrow \alpha' +$ hydride phase transformation at ~3 and 0.3 K/s, is shown in Fig. 26. All specimens that were cooled at the slower rate (Fig. 26b) exhibit fracture toughness values of ~10-15 MPa·m$^{1/2}$ at temperatures of ≤573 K and a brittle fracture mode (e.g., Fig. 27). At 673 K, specimens with ≤1400 wt ppm hydrogen have a ductile fracture mode and large toughness values (≥40 MPa·m$^{1/2}$). For temperatures of ≥473 K, the fracture toughness of the specimens cooled through the phase transformation at 3 K/s is considerably larger than that of the slow-cooled material.

The effect of hydrogen concentration and cooling rate through the temperature range of the $\beta \rightarrow \alpha' +$ hydride phase transformation on the morphology and distribution of hydrides in Zircaloy-2 specimens is illustrated in Figs. 28-32. For material cooled at the slow rate (~0.3 K/s), hydride precipitation occurs primarily at the periphery of the α' grains (Fig. 28), and the fracture path is coincident with this region (Fig. 29) in specimens tested at low temperatures (~373 K). Figure 30 shows the microstructure of material cooled at the higher rate (~3 K/s). Preferential fracture at the α-grain boundaries is not evident after impact at 473 K. SEM micrographs of Zircaloy-2 specimens with 600 and 227 wt ppm hydrogen that were cooled through the temperature range of the $\beta \rightarrow \alpha' +$ hydride phase transformation at rates of ~0.3 and 3.0 K/s, respectively, are shown in Figs. 31 and 32. The slow-cooling rate is conducive to the formation of relatively large hydride platelets (e.g., Fig. 31).

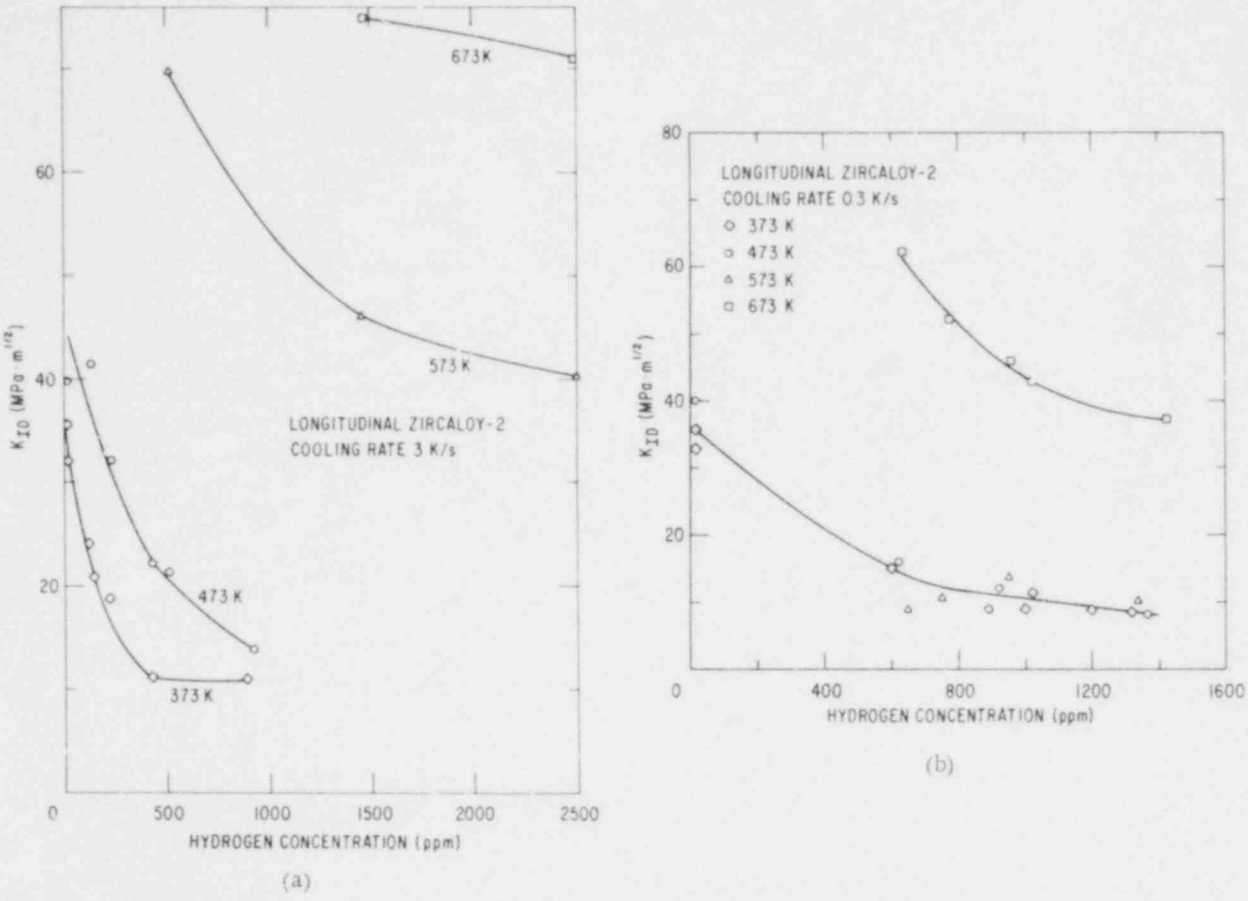

Fig. 26. Dynamic Fracture Toughness as a Function of Hydrogen Concentration in Zircaloy-2 Specimens with Longitudinal Texture at Several Temperatures between 373 and 673 K. The subsize Charpy specimens were cooled through the temperature range of the $\beta \rightarrow \alpha' +$ hydride phase transformation at rates of (a) 3 K/s and (b) 0.3 K/s. Impact velocity was 0.75 m/s. Neg. Nos. MSD-66180 and -66178.

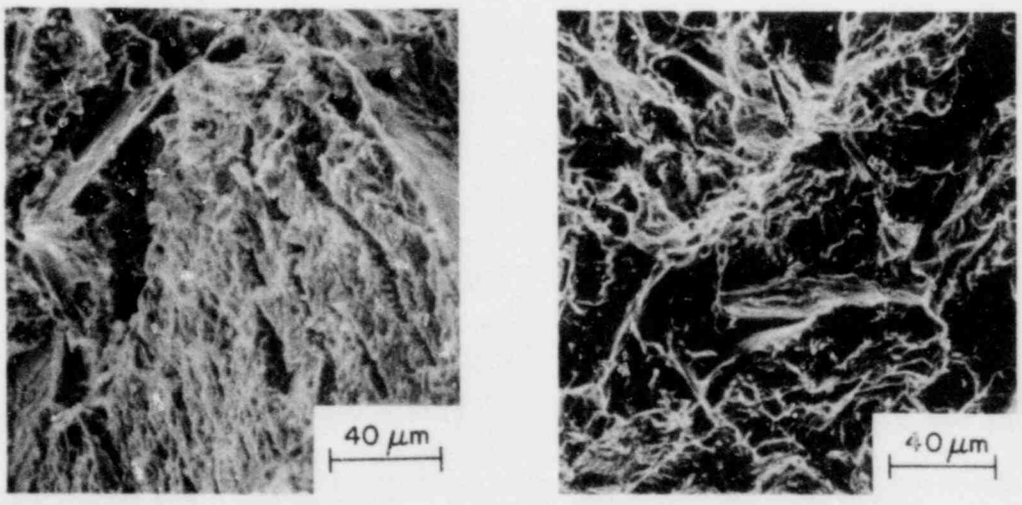

Fig. 27. SEM Fractographs of Longitudinal Zircaloy-2 Specimens with 600 wt ppm Hydrogen Which Indicate a Predominantly Brittle Fracture Mode after Impact Testing at (a) 373 and (b) 473 K. Specimens were cooled through the temperature range of the $\beta \rightarrow \alpha' +$ hydride phase transformation at a rate of ~0.3 K/s. Neg. Nos. MSD-66000 and -65998.

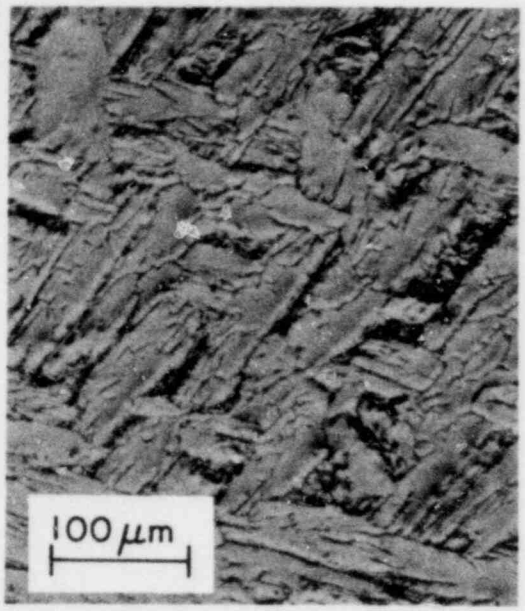

Fig. 28

Optical Micrograph of a Zircaloy-2 Specimen with 1000 wt ppm Hydrogen Which Shows Hydride Precipitation at the Periphery of the α' Grains. The specimen was cooled through the temperature range of the β→α' + hydride phase transformation at a rate of ~0.3 K/s. Neg. No. MSD-66001.

Fig. 29

Optical Micrograph of a Zircaloy-2 Specimen with 600 wt ppm Hydrogen Which Shows a Fracture Path along the Periphery of the α' Grains. The specimen was cooled through the temperature range of the β→α' + hydride phase transformation at a rate of ~0.3 K/s and impact tested at 373 K. Mag. 80X. ANL Neg. No. 306-80-225.

Fig. 30

Optical Micrograph of a Zircaloy-2 Specimen with 227 wt ppm Hydrogen Which Does Not Show Cracks along the Periphery of the α' Grains. The specimen was cooled through the temperature range of the $\beta \rightarrow \alpha' +$ hydride phase transformation at a rate of ~3 K/s (acicular structure) and impact tested at 473 K. Mag. 26X. ANL Neg. No. 306-80-226.

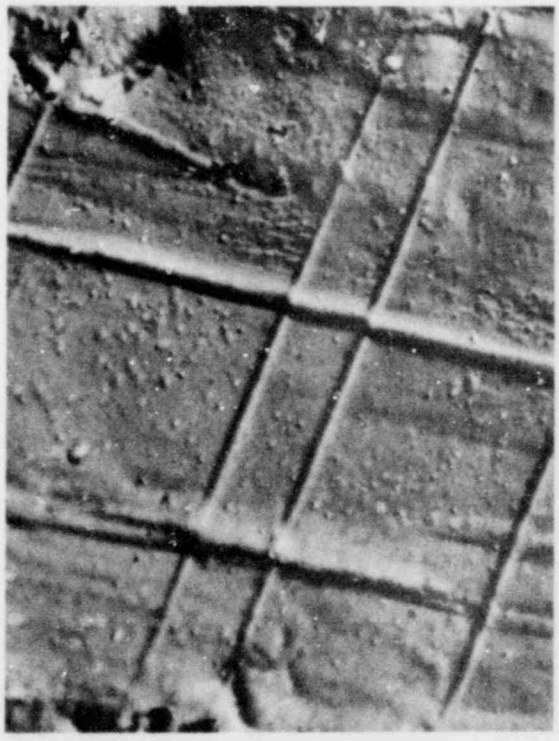

Fig. 31

SEM Micrograph of the Zircaloy-2 Specimen Depicted in Figs. 27a and 29 (600 wt ppm Hydrogen, 0.3 K/s) That Shows Fracture of Thick Hydride Plates by Deformation Twins in the Metal. Mag. ~1200X. ANL Neg. No. 306-80-227.

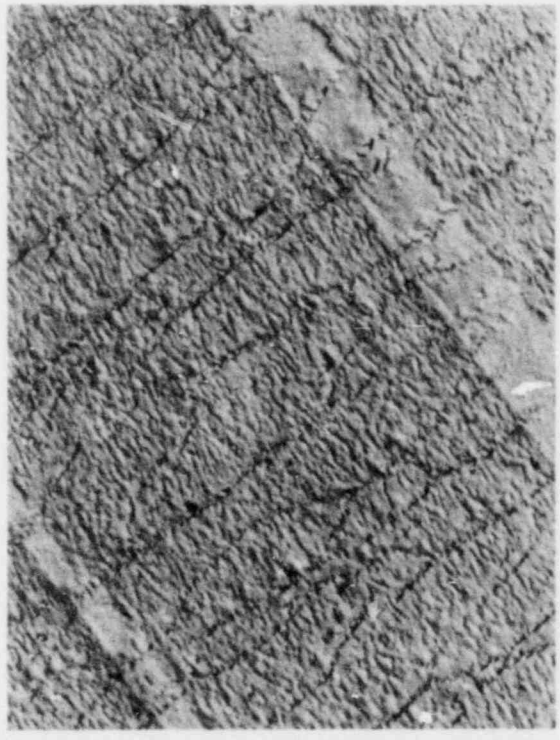

Fig. 32

SEM Micrograph of the Zircaloy-2 Specimen Depicted in Fig. 30 (227 wt ppm Hydrogen, 3 K/s) That Shows a Fine, Discontinuous Hydride Morphology. Deformation twins do not cause extensive microcracking of the discontinuous hydride phase. Mag. ~800X. ANL Neg. No. 306-80-228.

The hydride distribution and morphology produced by the two cooling rates could influence the dynamic toughness behavior, depicted in Fig. 26, in the following manner: As the test temperature increases, hydrogen dissolves in the matrix and the particle size decreases, while the distance between particles increases. For material with a more uniform distribution of hydrides (Fig. 26a), propagation of microcracks in the region between the hydride particles becomes more difficult as the toughness of the matrix and the fracture path length between particles increase. When hydrides are located primarily in the grain-boundary region (Fig. 26b), a relatively large increase in temperature (i.e., to ~600 K) is required to have a significant effect on interparticle fracture path, and, consequently, the dynamic fracture toughness is independent of temperature over the range of ~373 to 573 K.

The precipitation of zirconium hydrides from supersaturated solutions of hydrogen in zirconium[32-37] and zirconium alloys[36-40] has been studied extensively by optical and electron microscopy and x-ray and electron-diffraction techniques. In addition to alloy composition, hydrogen content, and cooling rate, the stress state in the material has a strong influence on the distribution and morphology of hydrides in zirconium alloys.[31,41-43]

C. Comparison of Embrittlement Characteristics of Oxygen and Hydrogen

The relative effect of oxygen and hydrogen on the dynamic fracture toughness of Zircaloy-2 is shown in Fig. 33. On the basis of atom fraction, oxygen has a greater effect on the impact properties of transformed β-phase Zircaloy at temperatures of ≤600 K. At higher temperatures, the influence of hydrogen on fracture toughness decreases markedly (Fig. 26).

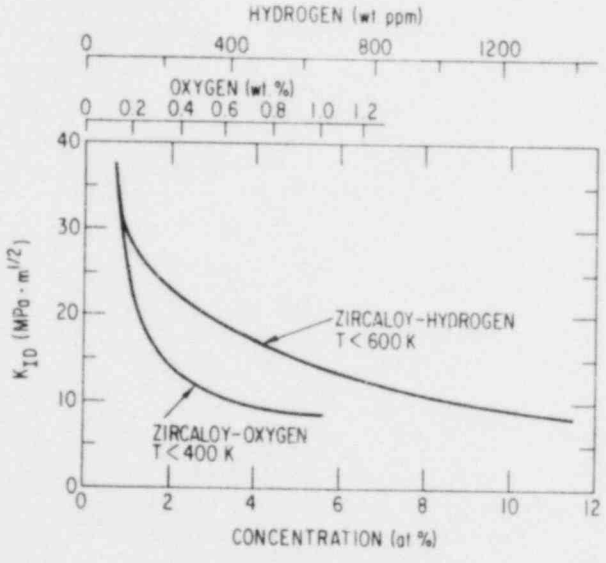

Fig. 33. Comparison of the Effect of Oxygen and Hydrogen on the Dynamic Fracture Toughness of Zircaloy at Temperatures of ≤400 and 600 K, Respectively

The smaller dependence of fracture toughness on hydrogen concentration, coupled with the fact that oxygen decreases the solubility of hydrogen in β-phase zirconium,[44,45] provides a rationale for the observation that the thermal-shock-failure properties of Zircaloy cladding, which was oxidized in steam at high temperatures, can be correlated with the thickness and oxygen content of the transformed β-phase layer,[5,46] although the tubes contain up to 2200 wt ppm hydrogen. When the cladding cools through the temperature range of the $\beta \rightarrow \alpha'$ phase transformation (~1450-1100 K) at a rate of ~5 K/s, oxygen partitioning occurs and the α' grains are enriched

in oxygen compared with the grain boundaries. Hydrogen tends to segregate to the grain-boundary regions during cooling because of the higher solubility in the β phase; however, during rapid cooling (~970 K/s) from ~850 K (due to the transition from film to nucleate boiling during flooding of the tube with water), either hydride precipitation is suppressed[5] or a fine hydride structure is produced[35] which cannot be easily resolved by optical or scanning-electron microscopy. Hydrogen or a fine hydride distribution in rapidly quenched Zircaloy cladding has a minimal effect on the thermal-shock-failure characteristics of the material. This observation is consistent with the effect of cooling rate on the fracture toughness of Zircaloy-hydrogen alloys.

Although the impact properties of Zircaloy-oxygen-hydrogen alloys (with >0.14 wt % oxygen and >25 wt ppm hydrogen) were not investigated, the dynamic fracture toughness of material containing high concentrations of both elements could be represented by a three-dimensional plot similar to Fig. 34, which shows the effect of these elements on the plastic deflection to the point of maximum load from diametral compression tests on Zircaloy cladding at 300 K.[5] As in the case of the diametral compression properties, it is unlikely that high concentrations of hydrogen (~100-1000 wt ppm) would result in a significant decrease in the fracture toughness of Zircaloy containing ≥0.4 wt % oxygen relative to the curve in Fig. 33.

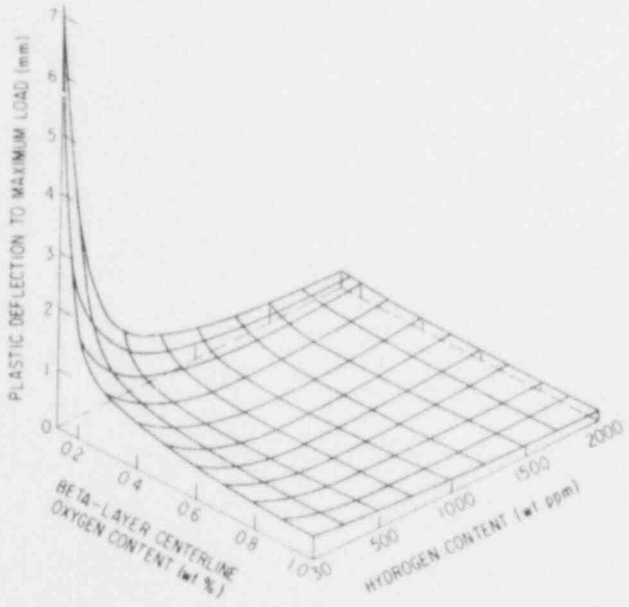

Fig. 34

Three-dimensional Representation of the Plastic Deflection to Maximum Load at 300 K Relative to the β-layer Centerline Oxygen Concentration and Hydrogen Content of Zircaloy-4 Cladding.[5] ANL Neg. No. 306-79-849.

IV. SUMMARY AND CONCLUSIONS

The impact properties of Zircaloy with ~0.13 to 1.3 wt % oxygen and ~10 to 2500 wt ppm hydrogen have been evaluated at temperatures between 373 and 823 K. Self-consistent criteria for the transition from ductile to brittle fracture relative to the temperature and oxygen concentration of the material were established on the basis of (a) total absorbed energy of ~1.3 x 10^4 J/m^2, (b) dynamic fracture toughness of ~10 MPa·$m^{1/2}$, (c) ductility index of ~0, (d) <25% of the fracture surface area with shear dimples, and (e) deflection angle of the deformed specimens of <5°. The type of alloy (e.g., Zircaloy-2 or -4), texture (i.e., specimen orientation in relation to the rolling direction of the material), and specimen geometry (notch versus fatigue precrack) had virtually no effect on the total absorbed energy and dynamic fracture toughness of specimens which exhibit a predominantly brittle fracture mode.

The influence of hydrogen concentration and the morphology and distribution of the hydride phase, produced by cooling the specimens through the temperature range of the $\beta \rightarrow \alpha' +$ hydride phase transformation at rates of ~0.3 and 3 K/s, on the impact properties of Zircaloy-2 with a longitudinal texture was investigated at temperatures between 373 and 673 K. Hydride precipitation in material cooled at the slower rate occurred primarily at the periphery of the α' grains and the fracture path coincided with this region in specimens that were tested at a low temperature (e.g., 373 K). Dynamic-fracture-toughness values for slow-cooled material with ≥600 wt ppm hydrogen ranged from ~10 to 15 MPa·$m^{1/2}$ at temperatures ≤573 K, whereas the material exhibited toughness values of ~40-60 MPa·$m^{1/2}$ at 673 K. Because of the fine, discontinuous hydride morphology and transgranular fracture of material that was cooled through the phase-transformation range at the higher rate, the fracture toughness values exhibited a strong dependence on temperature over the range of 373 to 573 K (e.g., ~10-60 MPa·$m^{1/2}$ for Zircaloy with ~1000 wt ppm hydrogen).

Based upon atom fraction, oxygen has a greater effect than hydrogen on the impact properties of transformed β-phase Zircaloy at temperatures between ~400 and 600 K. Consequently, information on the fracture toughness of Zircaloy-oxygen alloys at low temperatures is appropriate for use in analyses of the structural integrity of fuel rods which are subjected to high-temperature oxidation in steam during postulated accident situations in LWRs.

APPENDIX A

Analysis of Uncertainties in the Experimental Data

The uncertainty level for various measured quantities pertaining to the impact properties of Zircaloy-oxygen/hydrogen alloys has been evaluated. The uncertainty in the impact properties results from the normal random errors in the laboratory measurements and the effects of the local microstructure in the vicinity of the V-notch on crack propagation, which was discussed in Section II.

Temperature. The error in the temperature measurement in the impact tests, due to thermocouple calibration and the digital-readout instruments, is ±5 K.

Concentration of Oxygen and Hydrogen in the Zircaloy. The oxygen and hydrogen uptake by the impact specimens during the charging and homogenization period was determined by gravimetric measurements. The accuracy of the weight-change measurements was ±100 μg for a nominal specimen weight of ~8.8 g. Therefore, the uncertainty in the oxygen and hydrogen concentrations in the specimens is ±25 wt ppm. The hydrogen concentration of the specimens was also determined by inert-gas fusion analyses of the specimens after the impact tests.

Measurements of the Crack Length and Specimen Width (a/W Ratio). The crack length in fatigue-precracked specimens was obtained from the average of the crack lengths on the opposite surfaces of the specimen, i.e., $a = (a_1 + a_2)/2$. The accuracy of the actual measurement of a_1, a_2 and W was ±0.01 mm, and the uncertainty in the a/W ratio is ±5%.

Load Measurements. The sources of uncertainty in the load measurements result from random errors in the electronic measurement system [i.e., oscilloscope trace (±3%), analog to digital converter (±0.2%), analog plot on the X-Y recorder (±1% of full scale), and amplifier error due to static rather than dynamic calibration], as well as microstructural variations in the material in the vicinity of the V-notch, i.e., the orientation of α' platelets and the presence of a grain boundary below the notch. The error in the load values due to the electronic measurement system is small (±5%) in comparison with microstructural effects, which produce most of the variability in the experimental data.

Time Measurements. The maximum random error in the time measurements from the energy and load versus time traces on the oscilloscope is ±60 μs. Since the time to maximum load was greater than the rise time for the oscilloscope (125 μs), the load was not attenuated. The estimated error in the time values obtained from the Nova II computer systems is ± 2%.

Energy Measurements. Factors that contribute to the estimated random error in the impact energy of ±15% include: velocity of the crosshead at impact (±10%), oscilloscope readings (±3%), specimen cross-sectional area (±1%), and planimetric measurements of the area under the load-time curve (±1%) when this method is used to calculate the impact energy.

Fracture Toughness Measurements. In addition to the factors that contribute to the uncertainty in the load measurements, a deviation from plane-strain conditions and the absence of a fatigue precrack in specimens with low oxygen or hydrogen concentrations result in elastic-plastic (ductile) fracture, and, consequently, a significant overestimate of the dynamic fracture toughness for these specimens. From the standpoint of Zircaloy embrittlement by oxygen and hydrogen, the impact properties of as-received material at low temperatures and the alloys of Zircaloy with hydrogen and oxygen at high temperatures are not relevant, but the results are included for comparison.

Ductility Index. Because of the relatively large uncertainty in the crack initiation and propagation energies, the uncertainty in the values of the ductility index, which is the ratio of these quantities, is quite large, i.e., ±35%.

APPENDIX B

Summary of Impact-test Results

The results of the impact measurements on Zircaloy-oxygen and Zircaloy-hydrogen alloys are given in Tables B.1-B.7 and B.8-B.9, respectively. Results for notched and precracked Zircaloy-4/oxygen specimens with transverse texture are contained in Tables B.1 and B.2, respectively. Data for Zircaloy-4/oxygen specimens with a longitudinal texture are given in Table B.3. Information on the impact properties of Zircaloy-2/oxygen specimens with transverse and longitudinal textures is listed in Tables B.4 and B.5, respectively. Table B.6 provides information on the effect of cooling rate (~3 K/s) through the temperature range of the $\beta \rightarrow \alpha'$ phase transformation on the impact properties of longitudinal Zircaloy-4 specimens with ~0.13 wt % oxygen. Impact data for as-received Zircaloy-2 specimens with longitudinal and transverse textures are listed in Table B.7.

Impact results for longitudinal-texture Zircaloy-2/hydrogen specimens, which were cooled through the temperature range of the $\beta \rightarrow \alpha'$ + hydride phase transformation at rates of ~3 and 0.3 K/s, are given in Tables B.8 and B.9, respectively.

TABLE B.1. Impact Results[a] from Homogeneous Zircaloy-4/Oxygen Specimens with Transverse Texture[b]

Specimen Number	Oxygen, wt %	a/W	Temp., K	Load, kN		Time, μs			Energy/Area, 10^4 J/m^2			K_{ID}, MPa·m$^{1/2}$	Ductility Index
				Yield (P_{GY})	Max. (P_{max})	To Yield (t_{GY})	To Max. Load (t_m)	To Fracture (t_f)	Total (E_T/A)	To Max. Load (E_I/A)	Propagation (Ep/A)		
N5	0.13	0.2	298	0.96	1.48	800	3000	12600	27.8	11.40	17.40	47.8	1.4
N6	0.13	0.2	373	0.80	1.36	650	2800	14000	39.9	11.50	28.40	47.8	2.5
N9	0.13	0.2	373	0.92	1.32	800	3000	14000	37.0	11.80	25.20	48.3	1.8
N7[a]	0.13	0.2	473	0.76	1.16	800	4600	--	--	19.30	--	60.6	--
N8[a]	0.13	0.2	673	0.60	0.90	1200	7200	--	--	20.00	--	56.5	--
HN55	0.43	0.2	373	0.86	0.86	800	800	2600	2.7	1.00	1.70	11.8	1.7
HN58[c]	0.44	0.2	823	0.58	0.70	800	9600	--	--	23.30	--	59.9	--
HN60[c]	0.46	0.2	473	1.44	1.44	1600	1600	--	--	4.30	--	19.7	--
HN56	0.46	0.2	473	1.24	1.24	1400	1400	1600	2.6	2.60	0.00	17.0	0.0
HN51	0.53	0.2	473	1.32	1.32	1400	1400	1400	3.4	3.40	0.00	18.1	0.0
HN52[c]	0.56	0.2	673	1.16	1.24	1600	2400	--	--	6.50	--	27.1	--
HN53	0.60	0.2	673	1.20	1.40	1500	2800	2800	9.6	9.60	0.00	35.4	0.0
HN49	0.62	0.2	373	0.82	0.82	800	800	1000	1.5	1.00	0.50	11.2	0.5
HN50	0.62	0.2	473	0.92	0.92	1100	1100	1200	1.7	1.70	0.00	12.6	0.0
HN54[c]	0.62	0.2	823	0.30	0.52	600	7000	--	--	21.90	--		0.0
HN11[c]	0.72	0.2	673	1.16	1.24	1600	2000	--	--	5.60	--	24.1	--
HN16	0.77	0.2	473	0.96	0.96	800	800	1000	1.7	1.70	0.00	13.2	0.0
HN14	0.81	0.2	373	0.60	0.60	500	500	500	1.0	1.00	0.00	8.2	0.0
HN3	0.90	0.2	373	0.42	0.42	600	600	1600	0.7	0.50	0.20	6.3	0.4
HN4	0.90	0.2	473	0.54	0.54	600	600	2000	1.3	0.50	0.80	5.7	1.5
HN2	0.96	0.2	823	0.76	0.96	1350	1600	11000	16.7	3.00	13.70	13.0	4.6
HN1	1.00	0.2	673	0.92	0.92	1000	1000	1000	1.5	1.50	0.00	12.6	0.0
HN72	1.08	0.2	473	0.68	0.68	800	800	800	0.8	0.80	0.00	9.3	0.0
HN70	1.10	0.2	673	0.63	0.63	900	900	900	1.2	1.20	0.00	8.7	0.0
HN71	1.10	0.2	823	1.12	1.12	1400	1400	--	--	2.70	--	15.3	--
HN68	1.20	0.2	673	0.30	0.30	450	450	450	0.2	0.15	0.05	3.3	0.4
HN67	1.20	0.2	823	0.98	0.98	1225	1225	1225	2.3	2.30	0.00	13.4	0.0

[a] Impact velocity was 0.75 m/s.
[b] The subsize Charpy specimens were cooled through the temperature range of the β → α' phase transformation at a rate of ~3 K/s.
[c] Partial fracture.

TABLE B.2. Impact Results[a] from Precracked Zircaloy-4/Oxygen Specimens with Transverse Texture[b]

Specimen Number	Oxygen, wt %	a/W	Temp., K	Load, kN		Time, μs			Energy/Area, 10^4 J/m^2			K_{ID}, MPa·m$^{1/2}$	Ductility Index
				Yield (P_{GY})	Max. (P_{max})	To Yield (t_{GY})	To Max. Load (t_m)	To Fracture (t_f)	Total (E_T/A)	To Max. Load (E_I/A)	Propagation (E_p/A)		
H48	0.13	0.34	373	0.62	0.80	700	1700	16500	19.3	4.2	15.1	29.0	3.6
25	0.13	0.39	298	0.64	0.78	600	1500	9000	17.9	4.0	13.9	30.8	3.5
47	0.13	0.39	373	0.62	0.78	650	2200	10400	24.5	6.6	17.9	38.6	2.7
45[c]	0.13	0.42	473	0.48	0.56	700	1800	--	--	4.2	--	29.4	--
20[c]	0.13	0.42	673	0.32	0.53	600	8600	--	--	17.9	--	58.1	--
H46	0.13	0.51	373	0.37	0.47	900	1890	13520	15.9	3.5	12.4	25.2	3.5
H26	0.30	0.38	373	0.88	0.88	800	800	1600	2.6	1.4	1.2	19.3	0.8
H39	0.41	0.32	373	0.60	0.60	820	820	1840	1.8	1.0	0.8	11.3	0.8
H38	0.46	0.38	373	0.54	0.54	650	650	2000	1.6	1.0	0.6	11.9	0.6
H40	0.47	0.37	473	0.60	0.60	700	700	2000	2.2	1.0	1.2	12.8	1.3
H18	0.78	0.38	473	0.56	0.56	700	700	1720	1.7	0.9	0.8	12.3	0.9
H15	0.78	0.50	473	0.47	0.47	700	700	2460	2.9	1.0	1.9	14.6	1.9
H34	0.99	0.26	473	0.56	0.56	590	590	1280	0.8	0.6	0.2	9.0	0.4
H36	1.00	0.29	473	0.69	0.69	800	800	1545	1.6	1.0	0.6	12.0	0.6
HN5	1.16	0.45	673	0.44	0.46	850	1000	2500	2.7	1.4	1.3	14.1	1.0

[a] Impact velocity was 0.75 m/s.
[b] The subsize Charpy specimens were cooled through the temperature range of the β → α' phase transformation at a rate of ≈3 K/s.
[c] Partial fracture.

TABLE B.3. Impact Results[a] from Homogeneous Zircaloy-4/Oxygen Specimens with Longitudinal Texture[b]

Specimen Number	Oxygen, wt %	a/W	Temp., K	Load, kN		Time, μs			Energy/Area, 10^4 J/m^2			K_{ID}, MPa·m$^{1/2}$	Ductility Index
				Yield (P_{GY})	Max. (P_{max})	To Yield (t_{GY})	To Max. Load (t_m)	To Fracture (t_f)	Total (E_T/A)	To Max. Load (E_I/A)	Propagation (E_p/A)		
N14	0.13	0.20	298	1.08	1.56	900	2200	12000	19.4	8.2	11.2	38.4	0.85
N13	0.13	0.20	373	0.96	1.44	800	2400	15000	36.8	9.2	27.6	41.4	2.50
N16[c]	0.13	0.20	373	0.96	1.44	800	2600	14600	30.9	9.6	21.3	42.5	1.90
N15[c]	0.13	0.20	473	0.90	1.20	800	2800	--	--	9.0	--	40.3	--
N17[c]	0.13	0.20	473	0.76	1.12	900	2110	--	--	9.5	--	40.3	--
HN31[c]	0.41	0.20	673	0.88	0.98	1400	2200	--	--	5.0	--	23.7	--
HN28	0.44	0.20	373	1.08	1.08	1200	1200	3200	3.1	2.5	0.6	14.8	0.18
HN30	0.44	0.20	473	1.16	1.16	1000	1000	3400	4.0	2.0	2.0	15.9	1.00
HN12	0.52	0.20	373	0.72	0.72	885	885	2460	1.3	1.1	0.2	8.3	0.20
HN11[c]	0.55	0.20	673	0.88	1.16	1000	1800	--	--	4.3	--	22.4	--
HN10	0.56	0.20	473	0.82	0.82	1000	1000	1000	1.5	1.5	0.0	11.2	0.0
HN72[c]	0.61	0.20	673	0.98	1.16	1145	1720	--	--	5.0	--	24.7	--
HN9	0.64	0.20	373	0.60	0.64	800	1200	2400	2.4	1.8	0.6	15.9	0.50
HN39	0.70	0.20	373	0.52	0.52	820	820	4100	1.1	1.0	0.1	7.1	0.10
HN38	0.71	0.20	473	1.02	1.02	1225	1225	1225	2.0	2.0	0.0	14.0	0.00
HN42[c]	0.72	0.20	673	1.12	1.12	1635	1635	--	--	3.3	--	15.3	--
HN40	0.77	0.20	473	0.55	0.55	1125	1125	1385	1.2	1.0	0.2	7.5	0.12
HN45	0.80	0.20	673	1.08	1.08	1200	1200	1200	2.3	2.3	0.0	14.8	0.00
HN46	0.87	0.20	473	0.62	0.62	655	655	1230	1.0	0.9	0.1	8.5	0.15
HN47	0.91	0.20	673	0.84	0.84	920	920	1845	1.7	1.5	0.2	11.5	0.10
HN22	1.24	0.20	673	0.42	0.42	490	490	1640	0.6	0.4	0.2	5.8	0.50
HN23	1.24	0.20	823	0.38	0.38	920	920	1945	0.7	0.5	0.2	5.2	0.30
HN24	1.28	0.20	823	0.76	0.76	1025	1025	1895	1.6	1.3	0.3	10.5	0.20
H9[d]	0.59	0.38	473	0.51	0.51	735	735	3360	1.5	0.9	0.6	11.2	0.70
H50[e]	0.86	0.50	473	0.29	0.29	715	715	2150	0.9	0.5	0.4	8.9	0.80
H18[c]	1.24	0.34	673	0.56	0.56	940	940	3215	1.7	0.9	0.8	9.1	0.90
H53[c]	1.05	0.26	473	0.52	0.52	470	470	3235	1.7	0.5	1.2	8.5	2.50
H54[c]	0.98	0.52	673	0.66	0.66	1085	1190	5120	12.3	3.3	9.0	26.7	2.70

[a]Impact velocity was 0.75 m/s.
[b]The subsize Charpy specimens were cooled through the temperature range of the β → α' phase transformation at a rate of ~3 K/s.
[c]Partial fracture.
[d]Precracked.
[e]Sawcut.

TABLE B.4. Impact Results from Homogeneous Zircaloy-2/Oxygen Specimens with Transverse Texture[a]

Specimen Number	Oxygen, wt %	a/W	Temp., K	Load, kN		Time, μs			Energy/Area, 10^4 J/m^2			K_{ID}, MPa·m$^{1/2}$	Ductility Index
				Yield (P_{GY})	Max. (P_{max})	To Yield (t_{GY})	To Max. Load (t_m)	To Fracture (t_f)	Total (E_T/A)	To Max. Load (E_I/A)	Propagation (E_p/A)		
Velocity 1.50 m/s													
101[c]	0.13	0.32	298	0.60	0.84	200	300	1100	2.90	1.20	1.70	16.8	1.50
103[b,c]	0.13	0.30	473	0.80	0.86	450	500	--	--	2.30	--	22.1	--
H76[c]	0.37	0.35	473	0.74	0.79	350	500	3600	6.50	2.00	4.50	19.8	2.20
HN90[b]	0.56	0.20	473	1.40	1.64	700	800	3100	8.00	5.50	2.50	24.0	0.45
HN92[b]	0.58	0.20	673	1.32	1.44	650	750	--	--	4.00	--	20.1	--
CHN94[b]	1.10	0.20	473	0.48	0.72	250	300	450	2.25	2.00	0.25	16.9	0.13
CHN96[b]	1.10	0.20	673	0.80	0.88	260	400	--	--	1.50	--	15.3	--
CHN93[b]	1.10	0.20	823	0.88	1.00	550	750	--	--	2.50	--	14.3	--
Velocity 0.75 m/s													
CHN104	0.13	0.20	298	0.88	1.44	1000	2000	4000	7.80	6.90	0.90	31.0	0.29
A[c]	0.13	0.41	373	0.46	0.53	740	1065	9625	7.20	1.70	5.50	12.1	3.17
CHN105	0.13	0.20	373	0.88	1.28	1000	2200	9800	12.40	6.80	5.60	32.3	0.71
CHN102[c]	0.13	0.36	373	0.64	0.72	800	1200	10000	10.30	2.50	7.80	21.0	2.70
CH77[c]	0.36	0.44	373	0.46	0.53	735	940	9830	6.00	1.30	4.70	14.6	3.50
CH88[b,c]	0.37	0.40	473	0.52	0.56	600	800	--	--	1.20	--	15.1	--
CH73[c]	0.46	0.48	373	0.38	0.38	735	735	2660	2.30	0.70	1.60	11.1	2.00
CH74[c]	0.47	0.33	298	0.56	0.56	800	800	800	1.20	1.20	0.00	10.8	0.00
CH35[c]	0.50	0.29	373	0.66	0.66	860	860	2450	2.80	1.00	1.80	11.5	1.70
CH69[c]	0.50	0.35	473	0.90	0.90	850	900	5700	6.10	1.70	4.40	17.8	2.60
CH70[c]	0.53	0.55	373	0.48	0.48	940	940	2275	2.60	1.50	1.10	17.4	0.73
CH67[c]	0.62	0.44	373	0.43	0.43	685	685	1230	1.50	0.75	0.75	11.0	1.00
CH30[c]	0.65	0.54	373	0.23	0.23	410	410	755	0.60	0.30	0.30	8.1	1.10
CH63[c]	0.66	0.42	473	0.42	0.46	630	1000	4400	3.60	1.40	2.20	15.7	1.60
CH32[c]	0.84	0.39	473	0.38	0.38	510	510	1810	0.80	0.40	0.40	8.6	1.20
CH84[c]	0.90	0.38	473	0.67	0.67	785	785	1670	2.30	1.90	0.40	14.7	0.20
CH49[c]	0.90	0.51	373	0.43	0.43	540	540	1280	1.40	0.80	0.60	13.7	0.80
CH98	0.95	0.20	673	0.72	0.72	1000	1000	1200	1.50	1.50	0.00	9.9	0.00
CHN100[b]	0.94	0.20	823	0.72	0.84	1000	1200	--	--	1.80	--	11.5	--

[a]The subsize Charpy specimens were cooled through the temperature range of the $\beta \rightarrow \alpha'$ phase transformation at a rate of ~3 K/s.
[b]Partial fracture.
[c]Precracked.

TABLE B.5. Impact Results[a] from Homogeneous Zircaloy-2/Oxygen Specimens with Longitudinal Texture[b]

Specimen Number	Oxygen, wt %	a/W	Temp., K	Load, kN		Time, μs			Energy/Area, 10^4 J/m^2			K_{ID}, MPa·m$^{1/2}$	Ductility Index
				Yield (P_{GY})	Max. (P_{max})	To Yield (t_{GY})	To Max. Load (t_m)	To Fracture (t_f)	Total (E_T/A)	To Max. Load (E_I/A)	Propagation (E_p/A)		
8	0.13	0.20	298	0.84	1.13	900	1555	2870	4.3	4.0	0.3	23.8	0.07
9	0.13	0.20	373	0.70	1.17	740	2420	5120	8.5	7.3	1.2	35.7	0.16
11	0.13	0.20	373	0.80	1.18	860	2130	6270	8.0	6.3	1.7	32.1	0.26
10	0.13	0.20	473	0.72	1.09	900	3030	17360	20.4	9.4	11.0	39.8	1.17
13	0.42	0.20	298	0.55	0.55	780	780	2170	1.1	0.6	0.5	7.5	0.75
12	0.42	0.20	373	0.52	0.52	980	980	3250	1.2	0.9	0.3	7.2	0.32
15	0.44	0.20	473	1.04	1.04	1400	1400	3525	2.8	2.4	0.4	14.2	0.20
16	0.45	0.20	473	1.15	1.15	1400	1400	2050	3.2	3.1	0.1	15.7	0.04
14[c]	0.45	0.20	673	0.88	1.05	1390	2040	--	--	4.9	--	22.3	--
27[c]	0.60	0.20	673	0.84	1.09	1310	2125	--	--	4.9	--	21.7	--
28	0.72	0.20	373	0.72	0.72	820	820	1435	1.2	1.0	0.2	9.9	0.12
30	0.71	0.20	473	0.89	0.89	940	940	1845	1.9	1.4	0.5	12.2	0.30
29[c]	0.76	0.20	673	0.70	1.04	1025	1940	--	--	4.2	--	20.6	--
41	0.80	0.20	473	0.66	0.66	1170	1170	1635	1.4	1.3	0.1	9.0	0.08
44	0.80	0.20	673	0.82	0.82	1325	1325	1735	2.3	2.1	0.2	11.3	0.11
43[c]	0.82	0.20	823	0.76	0.98	1230	6960	--	--	22.3	--	57.0	--
42[c]	0.88	0.20	673	0.70	0.70	820	820	--	--	1.5	--	9.9	--
51	0.97	0.20	673	0.74	0.74	870	870	925	1.2	1.0	0.2	10.2	0.13
50	0.98	0.20	673	0.70	0.70	1225	1225	2360	1.9	1.5	0.4	9.6	0.23
47	1.00	0.20	473	0.72	0.72	920	920	2250	1.9	1.3	0.6	9.9	0.40
49	1.01	0.20	823	0.80	0.80	1475	1475	14750	10.2	2.5	7.7	11.0	3.07
18[d]	0.42	0.32	373	0.79	0.79	825	825	1740	3.9	1.6	2.3	14.9	1.46
67[d]	0.56	0.37	473	0.56	0.56	715	715	1535	2.3	1.0	1.3	12.0	1.29
45[c,d]	0.74	0.31	473	0.99	0.99	1165	1165	--	--	2.0	--	18.2	--
31	0.73	0.56	473	0.39	0.39	820	820	2725	3.0	1.1	1.9	14.7	1.61
32	0.77	0.50	373	0.26	0.26	620	620	2700	2.0	0.5	1.5	8.0	3.05
33	0.79	0.31	373	0.31	0.31	480	480	1740	0.6	0.3	0.2	5.6	0.62
46	0.83	0.28	473	0.48	0.48	870	870	2845	1.1	0.9	0.2	8.2	0.28
53	0.93	0.25	473	0.52	0.52	665	665	1760	1.0	0.7	0.3	8.2	0.51
52	0.94	0.52	473	0.36	0.36	975	975	1870	1.0	0.7	0.3	12.0	0.41

[a] Impact velocity was 0.75 m/s.
[b] The subsize Charpy specimens were cooled through the temperature range of the $\beta \rightarrow \alpha'$ phase transformation at a rate of ~3 K/s.
[c] Partial fracture.
[d] Precracked.

TABLE B.6. Impact Results[a] from Longitudinal-texture Zircaloy-4 Specimens in the As-received Condition and after Cooling through the Temperature Range of the $\beta \rightarrow \alpha'$ Phase Transformation at a Rate of ~3 K/s

Specimen Number	Oxygen, wt %	a/W	Temp., K	Load, kN		Time, μs			Energy/Area, 10^4 J/m^2			K_{ID}, MPa·m$^{1/2}$	Ductility Index
				Yield (P_{GY})	Max. (P_{max})	To Yield (t_{GY})	To Max. Load (t_m)	To Fracture (t_f)	Total (E_T/A)	To Max. Load (E_I/A)	Propagation (E_p/A)		
α -- As Received													
CN1[b]	0.13	0.20	298	1.30	1.92	500	1600	--	--	17.5	--	60.7	--
CN3[b]	0.13	0.20	373	0.96	1.52	250	2000	--	--	19.3	--	65.0	--
CN2[b]	0.13	0.20	473	0.95	1.44	350	2300	--	--	22.0	--	63.8	--
CN4[b]	0.13	0.20	673	0.60	0.98	300	3800	--	--	23.4	--	63.5	--
NC[c]	0.13	0.35	298	0.61	0.85	300	500	5000	11.0	2.0	9.0	19.5	4.4
α_s' -- He Cooled (3 K/s)													
4	0.13	0.20	298	1.20	1.64	400	1150	4150	18.0	10.0	8.0	45.1	0.8
5[b]	0.13	0.20	473	1.00	1.28	250	2000	--	--	26.0	--	73.6	--
6[b]	0.13	0.20	673	0.56	0.92	300	3300	--	--	19.6	--	57.9	--
1	0.13	0.34	298	0.86	0.96	400	700	4300	14.8	4.8	10.0	32.5	2.1
2[b]	0.13	0.37	473	0.56	0.70	250	600	--	--	7.7	--	39.9	--

[a] Impact velocity was 1.5 m/s.
[b] Partial fracture.
[c] Precracked.

TABLE B.7. Impact Results from As-received Zircaloy-2 Specimens (0.13 wt % Oxygen) with Longitudinal and Transverse Textures

Specimen Number	Velocity, m/s	a/W	Temp., K	Load, kN		Time, μs			Energy/Area, 10^4 J/m^2			K_{ID}, MPa·m$^{1/2}$	Ductility Index
				Yield (P_{GY})	Max. (P_{max})	To Yield (t_{GY})	To Max. Load (t_m)	To Fracture (t_f)	Total (E_T/A)	To Max. Load (E_I/A)	Propagation (E_P/A)		
Longitudinal Texture													
N3	1.50	0.20	77	1.60	2.20	400	1250	1250	16.0	14.0	2.0	57.0	0.14
N5	1.50	0.20	193	1.44	2.08	400	1250	3000	22.0	15.5	6.5	58.0	0.42
N1	1.50	0.20	298	1.36	1.84	550	1450	3400	26.5	15.0	11.5	53.0	0.77
N6[a]	1.50	0.20	373	1.20	1.52	400	2000	--	--	19.0	--	63.0	--
N2[a]	1.50	0.20	473	0.88	1.24	350	2500	--	--	20.0	--	61.0	--
N8[b]	1.50	0.28	298	0.91	1.17	300	500	4400	11.3	2.4	8.9	23.1	3.69
O[a,b]	1.50	0.28	473	0.69	0.91	300	500	--	--	3.7	--	27.1	--
N7	0.75	0.20	298	1.04	1.68	900	3600	10000	30.8	16.6	14.2	58.0	0.86
N8[a]	0.75	0.20	373	1.03	1.34	1230	4500	--	--	19.4	--	61.3	--
63[b]	0.75	0.21	298	0.85	1.04	900	1270	9830	9.5	2.6	6.9	18.2	2.61
62[b]	0.75	0.29	298	0.74	0.81	890	1200	11200	9.4	2.4	7.0	19.3	2.95
61[b]	0.75	0.18	373	0.91	1.04	1065	1720	16465	22.4	4.1	18.3	23.5	4.43
Transverse Texture													
CN1	1.50	0.20	298	1.60	2.00	500	1400	3750	25.0	16.0	9.0	51.9	0.56
CN3[a]	1.50	0.20	473	0.96	1.48	350	1650	--	--	14.0	--	51.5	--

[a]Partial fracture.
[b]Precracked.

TABLE B.8. Impact Results[a] from Longitudinal-texture Zircaloy-2/Hydrogen Specimens Which Were Cooled through the Temperature Range of the β → α' + Hydride Phase Transformation at a Rate of ~3 K/s

Specimen Number	Hydrogen, wt. ppm	a/W	Temp., K	Load, kN		Time, μs			Energy/Area, 10^4 J/m^2			K_{ID}, MPa·m$^{1/2}$	Ductility Index
				Yield (P_{GY})	Max. (P_{max})	To Yield (t_{GY})	To Max. Load (t_m)	To Fracture (t_f)	Total (E_T/A)	To Max. Load (E_I/A)	Propagation (E_P/A)		
LCHN11	10	0.20	373	0.80	1.18	860	2130	6,270	8.0	6.3	1.7	32.1	0.26
HL31	114	0.22	373	0.76	1.08	840	1535	4,300	6.0	3.8	2.2	24.0	0.57
HL33	147	0.22	373	0.68	1.05	700	1310	3,235	4.1	3.0	1.1	20.7	0.38
HL35	216	0.21	373	0.84	1.00	820	1145	2,500	2.9	2.5	0.4	18.8	0.18
HL21	424	0.20	373	0.81	0.81	880	880	2,660	2.0	1.3	0.7	11.1	0.50
HL25	884	0.25	373	0.70	0.70	760	760	2,540	1.7	1.1	0.6	11.0	0.46
LCHN10	10	0.20	473	0.72	1.09	900	3030	17,360	20.4	9.4	11.0	39.8	1.17
HL32	125	0.19	473	0.82	1.15	1020	3235	16,385	26.8	10.5	16.3	41.4	1.55
HL36	227	0.20	473	0.82	1.15	920	2250	9,625	14.7	6.6	8.1	32.2	1.21
HL22	422	0.25	473	0.66	0.90	715	1435	3,685	3.8	3.1	0.7	22.2	0.23
HL24	510	0.21	473	0.72	0.92	820	1475	6,145	5.4	3.1	2.3	21.4	0.76
HL26	920	0.22	473	0.95	0.95	1125	1125	2,665	2.9	2.4	0.5	13.8	0.23
HL23[b]	516	0.20	573	0.69	1.18	820	7535	--	--	27.0	--	69.6	--
HL27	1447	0.24	573	0.90	1.29	1065	3030	4,015	12.3	12.3	0	46.5	0
HL19	2500	0.20	573	1.01	1.55	1045	2745	3,810	11.3	10.7	0.6	40.2	0.05
HL28[b]	1466	0.21	673	0.79	1.39	1150	7540	--	--	31.5	--	74.8	--
HL20	2516	0.22	673	0.92	1.45	1145	6300	9,625	42.9	28.4	14.5	70.9	0.51

[a] Impact velocity was 0.75 m/s.
[b] Partial fracture.

TABLE B.9. Impact Results[a] from Longitudinal-texture Zircaloy-2/Hydrogen Specimens Which Were Cooled through the Temperature Range of the $\beta \rightarrow \alpha' +$ Hydride Phase Transformation at a rate of ~0.3 K/s

Specimen Number	Hydrogen, wt. ppm	a/W	Temp., K	Load, kN		Time, μs			Energy/Area, 10^4 J/m^2			K_{ID}, MPa·m$^{1/2}$	Ductility Index
				Yield (P_{GY})	Max. (P_{max})	To Yield (t_{GY})	To Max. Load (t_m)	To Fracture (t_f)	Total (E_T/A)	To Max. Load (E_I/A)	Propagation (E_P/A)		
1	600	0.20	373	0.63	0.67	685	870	2,180	2.3	1.5	0.8	14.9	0.52
3	1000	0.20	373	0.63	0.63	685	685	1,270	1.5	1.0	0.5	8.7	0.51
4	1015	0.20	373	0.79	0.79	800	800	3,070	2.1	1.3	0.8	10.8	0.61
5	1200	0.20	373	0.68	0.68	675	675	1,720	1.4	0.9	0.5	9.3	0.60
17	1320	0.18	373	0.61	0.61	585	585	2,200	0.9	0.7	0.2	8.4	0.32
2	610	0.18	473	0.68	0.84	735	1025	9,135	4.9	1.9	3.0	15.5	1.60
11	878	0.18	473	0.65	0.65	840	840	4,120	3.5	1.2	2.3	8.5	2.00
14	930	0.23	473	0.47	0.60	510	820	4,400	3.6	1.2	2.4	12.2	2.00
18	1360	0.19	473	0.60	0.60	575	575	2,130	1.1	0.7	0.4	8.2	0.50
8	655	0.24	573	0.59	0.59	820	820	10,250	7.4	1.2	6.2	9.0	5.30
7	750	0.21	573	0.52	0.62	635	860	10,240	6.0	1.1	4.9	10.5	4.50
13	940	0.21	573	0.60	0.70	600	1000	10,400	6.4	1.5	4.9	13.8	3.40
15	1325	0.20	573	0.74	0.74	830	830	2,255	1.7	1.3	0.4	10.1	0.32
10[b]	661	0.22	673	0.53	0.92	820	7535	--	--	21.2	--	62.0	--
9[b]	770	0.23	673	0.52	0.86	820	6065	--	--	17.4	--	52.2	--
12[b]	955	0.18	673	0.57	0.88	740	4750	--	--	12.7	--	46.1	--
6[b]	1027	0.32	673	0.44	0.66	735	4505	--	--	10.6	--	42.5	--
16[b]	1230	0.18	573	0.56	0.90	820	3440	--	--	8.8	--	36.9	--

[a] Impact velocity was 0.75 m/s.
[b] Partial fracture.

ACKNOWLEDGMENTS

We wish to acknowledge the contributions of W. K. Soppet and R. H. Lee in performing the experimental work. The specimens were analyzed for hydrogen by F. L. Williams. We are grateful to F. A. Nichols, D. G. Westlake, and M. L. Picklesimer for helpful discussions. This work was sponsored by the Division of Water Reactor Safety Research of the U. S. Nuclear Regulatory Commission.

REFERENCES

1. D. T. Ramani, *Stress and Deflection Analysis of a Typical PWR Fuel Assembly Due to Seismic and Maximum Hypothetical LOCA Loading Conditions*, 4th Inter. Conf. on Structural Mechanics in Reactor Technology, San Francisco, August 15-19, 1977, T. A. Jaeger and B. A. Boley, Eds., CECA, CEE, CEEA, Luxembourg, p. D4/1 (1977).

2. H. Nuno, M. Mizuta, and N. Tsumura, *Development of Advanced Method for Fuel Seismic Analysis*, ibid, p. D4/6.

3. R. L. Grubb and B. F. Saffell Jr., *Non-Linear Lateral Mechanical Response of Pressurized Water Reactor Fuel Assemblies*, 77-WA/DE-18, Amer. Soc. of Mech. Eng., New York (December 1977).

4. R. L. Grubb, *Pressurized Water Reactor Lateral Core Response Routine, FAMREC (Fuel Assembly Mechanical Response Code)*, NUREG/CR-1019, EG&G Idaho, Inc. (September 1979).

5. H. M. Chung and T. F. Kassner, *Embrittlement Criteria for Zircaloy Fuel Cladding Applicable to Accident Situations in Light-Water Reactors: Summary Report*, Argonne National Laboratory Report NUREG/CR-1344, ANL-79-48 (January 1980).

6. R. L. Grubb, *LWR Fuel Rod Post Subcooled Blowdown Scoping Analysis*, NUREG/CR-1568, EG&G Idaho, Inc. (July 1980).

7. *Light-water-reactor Safety Research Program: Quarterly Progress Report, July-September 1977*, Sec. III, "Mechanical Properties of Zircaloy Containing Oxygen," Argonne National Laboratory Report ANL-78-3 (1978).

8. *Light-water-reactor Safety Research Program: Quarterly Progress Report, October-December 1977*, Sec. III, "Mechanical Properties of Zircaloy Containing Oxygen," Argonne National Laboratory Report ANL-78-25, NUREG/CR-0089 (1978).

9. *Light-water-reactor Safety Research Program: Quarterly Progress Report, January-March 1978*, Sec. III, "Mechanical Properties of Zircaloy Containing Oxygen," Argonne National Laboratory Report ANL-78-49, NUREG/CR-0201 (1978).

10. *Light-water-reactor Safety Research Program: Quarterly Progress Report, April-June 1978*, Sec. III, "Mechanical Properties of Zircaloy Containing Oxygen," Argonne National Laboratory Report ANL-78-77, NUREG/CR-0423 (1978).

11. *Light-water-reactor Safety Research Program: Quarterly Progress Report, July-September 1978*, Sec. III, "Mechanical Properties of Zircaloy Containing Oxygen," Argonne National Laboratory Report ANL-78-107, NUREG/CR-0547 (1978).

12. *Light-water-reactor Safety Research Program: Quarterly Progress Report, October-December 1978*, Sec. III, "Mechanical Properties of Zircaloy Containing Oxygen," Argonne National Laboratory Report ANL-79-18, NUREG/CR-0828 (1978).

13. A. M. Garde, H. M. Chung, and T. F. Kassner, *Uniaxial Tensile Properties of Zircaloy Containing Oxygen: Summary Report*, Argonne National Laboratory Report ANL-77-30 (June 1977).

14. H. M. Chung and T. F. Kassner, *Deformation Characteristics of Zircaloy Cladding in Vacuum and Steam Under Transient-Heating Conditions: Summary Report*, Argonne National Laboratory Report ANL-77-31, NUREG/CR-0344 (July 1978).

15. W. F. Brown, Jr. and J. B. Srawley, *Plane Strain Crack Toughness Testing of High Strength Metallic Materials*, ASTM STP 410, 1 (1967).

16. Instruction Manual for Dynatup Model 500 Impact-Data Readout System, Effects Technology, Inc., Santa Barbara, CA.

17. W. L. Server and D. R. Ireland, *Nonstandard Test Techniques Utilizing the Instrumented Charpy and Izod Tests*, ASTM STP 563, 74 (1974).

18. D. R. Ireland, Effects Technology, Santa Barbara, CA, personal communication (September 1977).

19. *MATRO - Version II, A Handbook of Materials Properties for Use in the Analysis of Light-Water Reactor Fuel Rod Behavior*, NUREG/CR-0497, TREE-1280, EG&G Idaho, Inc., p. 268 (February 1979).

20. M. L. Picklesimer, *Anodizing for Controlled Microstructural Contrast by Color*, Microscope 15, 472 (1967).

21. D. R. Ireland, W. L. Server, and R. A. Wullaert, Preliminary Topical Report No. 75-43, Effects Technology, Inc., Santa Barbara, CA (1975).

22. D. R. Ireland, *Critical Review of Instrumented Impact Testing*, paper 5, presented at Dynamic Fracture Toughness Conf., London, July 1976.

23. P. K. Mallick and L. J. Broutman, *Static and Impact Properties of Laminated Hybrid Composites*, J. Test. Eval. 5(3), 190 (1977).

24. P. W. R. Beaumont, P. G. Riewald, and C. Zweban, *Methods for Improving the Impact Resistance of Composite Material*, ASTM STP 568, 134 (1975).

25. G. F. Slattery, *The Terminal Solubility of Hydrogen in Zirconium Alloys between 30 and 400°C*, J. Inst. Met. 95, 43-47 (1967).

26. A. Sawatzky and B. J. S. Wilkins, *Hydrogen Solubility in Zirconium Alloys Determined by Thermal Diffusion*, J. Nucl. Mater. 22, 304-310 (1967).

27. J. J. Kearns, *Terminal Solubility and Partitioning of Hydrogen in the Alpha Phase of Zirconium, Zircaloy-2, and Zircaloy-4*, J. Nucl. Mater. 22, 292-303 (1967).

28. D. G. Westlake, *Initiation and Propagation of Microcracks in Crystals of Zirconium-Hydrogen Alloys*, ASM Trans. 56, 1 (1963).

29. D. Hardie, *The Importance of the Matrix in Hydride Embrittlement of Zirconium*, L'Hydrogène dans les Metaux, Congres International 2, 497-500 (1972).

30. C. E. Ells, S. B. Dalgaard, W. Evans, and W. R. Thomas, *Development of Zirconium-Niobium Alloys,* Proc. Third Intl. Conf. on Peaceful Uses of Atomic Energy, Vol. 9, pp. 91-99 (1964).

31. W. R. Thomas, S. B. Dalgaard, W. Evans, V. Fidleris, G. W. Parry, and P. A. Ross-Ross, *Irradiation Experience with Zircaloy-2,* ibid, pp. 80-87.

32. J. P. Langeron and P. Lehr, *Preparation de gros cristaux de zirconium et determination de l'orientation des precipites d'hydaure de zirconium,* Rev. Metall. 58, 901-906 (1958).

33. D. G. Westlake and E. S. Fisher, *Precipitation of Zirconium Hydride in Alpha Zirconium Crystals,* Trans. Am. Inst. Min. Metall. Pet. Eng. 224, 254-258 (1962).

34. J. E. Bailey, *Electron Microscope Observations on the Precipitation of Zirconium Hydride in Zirconium,* Acta Met. 11, 267-280 (1963).

35. D. G. Westlake, *Deposition of Hydrogen in Quenched Zirconium-Hydrogen Alloys,* J. Nucl. Mater. 16, 215-219 (1965).

36. D. G. Westlake, *The Habit Planes of Zirconium Hydride in Zirconium and Zircaloy,* J. Nucl. Mater. 26, 208-216 (1968).

37. J. S. Bradbrook, G. W. Lorimer, and N. Ridley, *The Precipitation of Zirconium Hydride in Zirconium and Zircaloy-2,* J. Nucl. Mater. 42, 142-160 (1972).

38. N. Ridley, K. G. Caulkin, and G. W. Lorimer, *Zirconium Hydride Precipitation in Zircaloy-2,* L'Hydrogène dans les Metaux, Congres International 2, 484-488 (1972).

39. V. S. Arunachalam, B. Lehtinen, and G. Östberg, *The Orientation of Zirconium Hydride on Grain Boundaries in Zircaloy-2,* J. Nucl. Mater. 21, 241-248 (1967).

40. D. O. Northwood, *Hydrides in Zirconium-2.5 wt % Niobium Alloy Pressure Tubing,* J. Nucl. Mater. 78, 112-116 (1978).

41. M. R. Louthan, Jr. and R. P. Marshall, *Control of Hydride Orientation in Zircaloy,* J. Nucl. Mater. 9, 170-184 (1963).

42. M. R. Louthan, Jr. and C. L. Angerman, *The Influence of Stress on the Hydride Habit Plane in Zircaloy-2,* Trans. Metall. Soc. AIME 236, 221-222 (1966).

43. C. J. Simpson, O. A. Kupcis, and D. V. Leemans, *Hydride Reorientation and Fracture in Zirconium Alloys,* Zirconium in the Nuclear Industry, A. L. Lowe, Jr. and G. W. Parry, Eds., ASTM-STP 633, pp. 630-642 (1977).

44. K. P. Singh and J. Gordon Parr, *Hydrogen Solubility in Zr-O Alloys,* Trans. Faraday Soc. 59, 2248-2255 (1963).

45. C. Roy, *An Experiment to Clarify the Effect of Dissolved Oxygen on the Terminal Solubility of Hydrogen in Zirconium,* J. Nucl. Mater. 13, 275-277 (1964).

46. S. Majumdar, *Modeling of Crack Growth in Oxidized Zircaloy Cladding During Thermal-shock Conditions,* Argonne National Laboratory Report ANL-78-44, NUREG/CR-0136 (May 1978).

Distribution for NUREG/CR-1408 (ANL-80-14)

Internal:

W. E. Massey
J. A. Kyger
B. R. T. Frost
R. W. Weeks
P. B. Abramson
L. Baker
H. M. Chung
J. B. Wozniak
A. M. Garde (6)
T. F. Kassner (24)
S. Majumdar
F. A. Nichols
E. M. Stefanski (2)
A. B. Krisciunas
ANL Contract File
ANL Libraries (3)
TIS Files (3)

External:

USNRC, Washington, for distribution per R3 (375)
DOE-TIC (2)
Manager, Chicago Operations and Regional Office, DOE
Chief, Office of Patent Counsel, DOE-CORO
President, Argonne Universities Association, Argonne, Ill.
Materials Science Division Review Committee:

- E. A. Aitken, General Electric Co., 310 DeGuigne Drive, Sunnyvale, Calif. 94086
- G. S. Ansell, Rensselaer Polytechnic Inst., Troy, N. Y. 12181
- R. W. Balluffi, Massachusetts Inst. of Technology, Cambridge, Mass. 02139
- R. J. Birgeneau, Massachusetts Inst. of Technology, Cambridge, Mass. 02139
- S. L. Cooper, The University of Wisconsin, Madison, Wis. 53706
- C. Laird, University of Pennsylvania, Philadelphia, Pa. 19174
- M. T. Simnad, General Atomic, P. O. Box 81608, San Diego, Calif. 92138
- C. T. Tomizuka, The University of Arizona, Tucson, Ariz. 85721
- A. R. C. Westwood, Martin Marietta Labs., 1450 S. Rolling Rd., Baltimore, Md. 21227